

**INCORPORATING RUBBLE MOUND JETTIES IN ELLIPTIC HARBOR WAVE
MODELS**

A Thesis

by

JIANFENG ZHANG

Submitted to the Office of Graduate Studies of
Texas A&M University
in partial fulfillment of the requirements for the degree of

MASTER OF SCIENCE

May 2007

Major Subject: Ocean Engineering

**INCORPORATING RUBBLE MOUND JETTIES IN ELLIPTIC HARBOR WAVE
MODELS**

A Thesis

by

JIANFENG ZHANG

Submitted to the Office of Graduate Studies of
Texas A&M University
in partial fulfillment of the requirements for the degree of
MASTER OF SCIENCE

Approved by:

Co-Chairs of Committee,	Vijay Panchang Patrick Lynett
Committee Members,	Billy Edge Achim Stössel
Head of Department,	David V. Rosowsky

May 2007

Major Subject: Ocean Engineering

ABSTRACT

Incorporating Rubble Mound Jetties in Elliptic Harbor Wave

Models. (May 2007)

Jianfeng Zhang, B.E., Hohai University

Co-Chairs of Advisory Committee: Dr. Vijay Panchang
Dr. Patrick Lynett

Simulation models based on the elliptic mild or steep slope wave equation are frequently used to estimate wave properties needed for the engineering calculations of harbors. To increase the practical applicability of such models, a method is developed to include the effects of rubble mound structures that may be present along the sides of entrance channels into harbors.

The results of this method are found to match those of other mathematical models (i.e. parabolic approximation & three-dimensional solution) under appropriate conditions, but they also deviate from results of parabolic approximations in some cases because dissipation can create angular scattering. Comparison with hydraulic model data also shows that this approach is useful for designing pocket wave absorbers that are used to reduce wave heights in entrance channels.

ACKNOWLEDGEMENTS

First and foremost, I would like to thank my advisor, Dr. Panchang. He has provided me with many brilliant ideas over the past two years, which has really helped me to discover deeply my knowledge. Then, I thank Dr. Lynett, who gave me much help in the study for my thesis. And I also thank my committee members, Dr. Edge and Dr. Stössel for their guidance and support throughout the course of this research.

Thank you also to Dr. Zeki and Dr. Li, who gave me some technical advice when I studied my thesis research. I also want to extend my gratitude to my friends, the department faculty and staff for making my time at Texas A&M University a great experience.

Finally, thank you to my mother and father for their encouragement and to my wife for her patience and love.

TABLE OF CONTENTS

	Page
ABSTRACT	iii
ACKNOWLEDGEMENTS	iv
TABLE OF CONTENTS	v
LIST OF FIGURES	vii
CHAPTER	
I INTRODUCTION	1
Background	1
Previous Work	4
Scope of Present Work	6
II PERFORMANCE OF ELLIPTIC MODEL IN INLET	7
III METHODOLOGY	16
Mathematical Background	16
Mathematical Formulation for Dissipation	17
Solution of the Mild-slope Equation with Dissipation	22
IV VALIDATION AGAINST OTHER MATHEMATICAL SOLUTIONS	30
Elementary Test	30
Pocket Wave Absorber	32
Straight Channel Bounded by Rubble Mound Jetties	35
Other Simulations	38
V SIMULATIONS NEAR POCKET ABSORBER IN PENTWATER HARBOR	43
VI CONCLUDING REMARKS	55

	Page
REFERENCES	57
VITA	62

LIST OF FIGURES

FIGURE	Page
1 Pocket wave absorber at Pentwater, Michigan	3
2 Pocket absorber configurations	4
3 Schematic diagram of inlet	8
4 Wave train normally incident to inlet; $kb = 6$, $kl = 30$ (Top: analytical method (Dalrymple and Martin 2000); bottom: present elliptic model)	10
5 Wave train incident at 45° to Inlet; $kb = 6$, $kl = 30$ (Top: analytical method (Dalrymple and Martin 2000); bottom: present elliptic model)	11
6 Plane view of instantaneous water surface elevation in rectangular channel; ocean at left, bay at right (Top: analytical method (Dalrymple and Martin 2000); bottom: present elliptic model)	12
7a Decay of wave height along channel centerline; $\gamma = 1 \text{ m}^{-1}$, $kb = 7.32$, $kl = 73.2$ (Analytical method (Dalrymple and Martin 2000))	12
7b Decay of wave height along channel centerline; $\gamma = 1 \text{ m}^{-1}$, $kb = 7.32$, $kl = 73.2$ (Present elliptic model)	13
8 Wave height comparison in the straight channel with dissipation for normally incident wave, reflection coefficient = 0.55 (Top: parabolic approximation (Melo and Guza 1991a); bottom: elliptic model incorporating the reflection coefficients)	14
9 Wave height comparison in narrow circular channel, with dissipation for normally incident wave, reflection coefficient = 0.4 (Top: parabolic approximation (Melo and Gobbi 1998); bottom: elliptic model incorporating reflection coefficients)	15
10 Definition sketch for jetty modeling	20
11 Harbor wave model domain; definition sketch	25
12 Non-linear convergence of the elliptic model	29

FIGURE	Page
13	Wave field in and around region of strong damping31
14	Wave field in and around region of weaker damping31
15	Wave field in and around region of weaker damping and 30^0 angle of incidence32
16a	Wave amplitude comparison in a channel with two pocket wave absorbers (3D model (Sulisz 2005))33
16b	Wave amplitude comparison in a channel with two pocket wave absorbers (present elliptic model)34
17	Modeled (normalized) wave amplitudes34
18	Straight channel model domain (after Melo and Guza 1991a)36
19	Wave height comparison for $\theta=0^0$. (Top: parabolic approximation (Melo and Guza 1991a); bottom: present elliptic model)37
20	Wave height comparison for $\theta=10^0$. (Top: parabolic approximation (Melo and Guza 1991a); bottom: present elliptic model)37
21	Wave height comparison in narrow circular channel, no dissipation. (Top: parabolic approximation (Melo and Gobbi 1998); bottom: present elliptic model)39
22	Wave height comparison in wide circular channel, no dissipation. (Top: parabolic approximation (Melo and Gobbi 1998); bottom: present elliptic model)40
23	Wave height comparison in narrow circular channel, with dissipation. (Top: parabolic approximation (Melo and Gobbi 1998); bottom: present elliptic model)41
24	Wave height comparison in wide circular channel, with dissipation. (Top: parabolic approximation (Melo and Gobbi 1998); bottom: present elliptic model)42
25	Pentwater Harbor entrance channel model (depth in m)44

FIGURE	Page
26 Pentwater entrance channel, hydraulic model gauge locations (numbered dots) and bathymetry (depth in m)	45
27 Modeled wave height comparison	46
28 Hydraulic and numerical model sea surface snapshot (top two panels) and numerical model phase diagram (bottom panel) for normally-incident wave	49
29 Hydraulic and numerical model sea surface snapshot (top two panels) and numerical model phase diagram (bottom panel) for oblique wave incidence	50
30 Wave height comparison, $H_i = 1\text{ m}$, $T = 5\text{ s}$	51
31 Wave height comparison, $H_i = 2\text{ m}$, $T = 7\text{ s}$	52
32 Modeled wave heights for alternative entrance channel configurations	54

CHAPTER I

INTRODUCTION

Background

Engineers frequently utilize computational modeling tools. These models include PHAROS, EMS, STWAVE, SWAN, CGWAVE, REFDIF and BOUSS-2D, which are commonly to be used to solve the practical coastal engineering problems. Many designers use an elliptic wave model (e.g. EMS, CGWAVE, PHAROS) to estimate the desired wave properties when they work on the design or modification of harbors. This model is based on the two-dimensional elliptical mild-slope wave equation. Originally, in this elliptical equation, wave properties such as refraction, diffraction and reflection were present. These properties are commonly induced by coastlines, structures and bathymetry in domains of arbitrary shapes for the entire range of practical wave condition. Later, additional wave properties, such as wave-current (Chan et al. 2005), wave breaking (Zhao et al. 2001), floating docks (Li et al. 2005), and steep-slope effects (Chandrasekara and Cheung 1997) have also been considered. Some elliptic wave models were developed and applied in many practical harbor problems, e.g. Ste. Therese de Gaspe Harbor, Kahului Harbor, Morro Bay Harbor, Venice Lagoon, Los Angeles/Long Beach Harbor, Barbers Point Harbor, etc. (Tang et al. 1999; Okihiro and Guza 1996; Thompson and Demirbilek, 2002; Thompson et al. 2002; Panchang and Demirbilek 2001; Mattioli 1996; Kostense et al. 1988; Bova et al. 2000; Zubier et al. 2003; and others).

As we know, navigation channels are usually constructed to connect small bays or lagoons to the ocean. But, the channels are not always satisfactory for navigation because they can create some severe wave conditions. Therefore, the design of these channels is important in the field of coastal engineering. One way commonly used to warrant the integrity and navigability of such channels is to protect them with rubble-mound jetties along their sides. How do these jetties work on the improvement of the channel? Firstly, they are built to prevent cross-channel sediment transport. Secondly, they prevent erosion along the sides when the channel is bounded by land on either side. Lastly, since they are rubble-mound structures, they can also partly dissipate high wave energy that could adversely affect navigation (e.g. Melo and Guza 1991*a*; 1991*b*).

However, in some cases, we cannot place a rubble-mound structure along the channel length. It is not suitable because it shortens the effective width of the navigable waterway which could cause navigation problems. There are alternative methods of wave attenuation to be considered. One method is to provide local expansions in the waterway. Stones are placed in the expansions to provide a rough, porous sloping surface. This surface is used to dissipate wave energy. And the remainder of the channel side is much smoother than the rubble mound boundary (local expansions filled with stones). This configuration has been referred to as “Pocket Wave Absorbers” by Thompson et al. (2004; 2005). Similar arrangements are called “Side Porous Caves” by Sulisz (2005). The locations of pockets which are installed are variable. In some instances they are located at the landward end of the channel, while the other cases they are situated more on the ocean side. Moreover, single or double pockets can be based on

practical project requirements. An example of a pair of a symmetric Pocket Wave Absorber at Pentwater, Michigan is shown in Figure 1.



Fig. 1. Pocket wave absorber at Pentwater, Michigan

Furthermore, several other configurations of Pocket Wave Absorber are possible (Fig. 2), such as two asymmetric pockets, a double-length single pocket, etc. In the channel, the properties of the rubble-mound sections, such as the length, the width, or the location will affect wave heights. For some cases, wave reflections can occur and the large waves can be found on the up-wave side of the pockets. This can sometimes cause navigation problems. Therefore, proper estimation of the effect of the rubble mound on the wave properties is a critical importance in obtaining optimum design. Little or no guidance for designing pocket wave absorber is available. This has been noted by Thompson et al. (2005) while they were performing engineering work for entrance channels in the Great Lakes region.

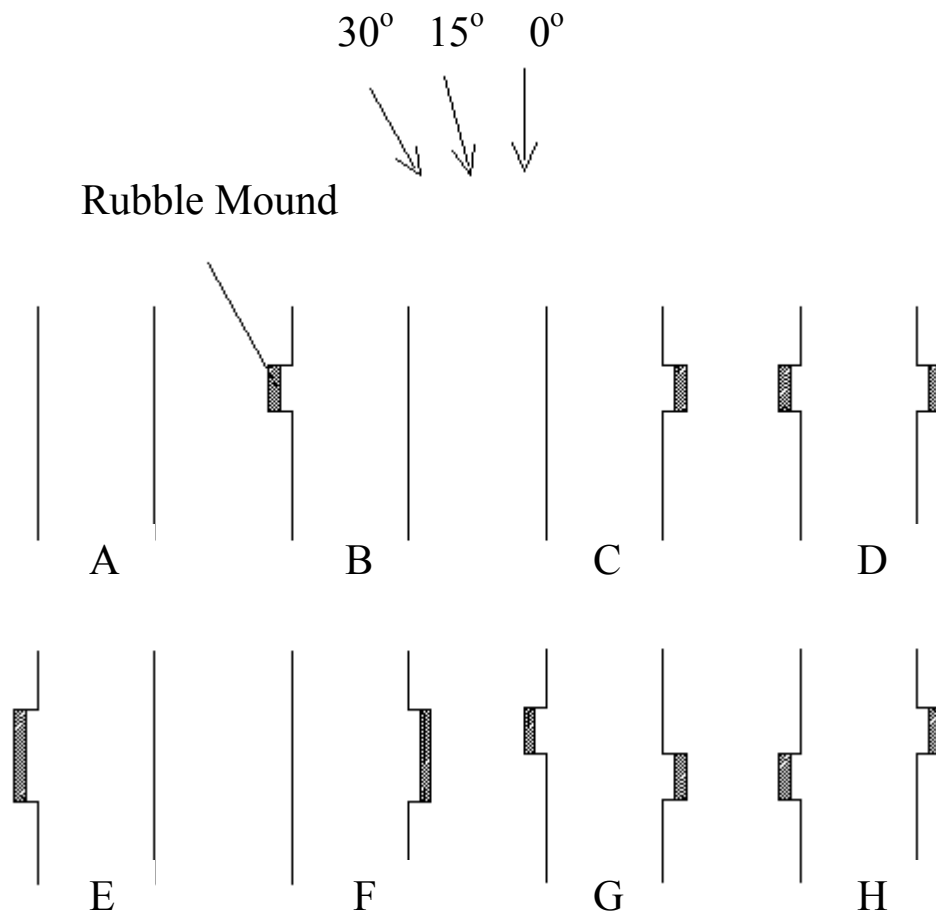


Fig. 2. Pocket absorber configurations

Previous Work

The mild-slope wave model is frequently used for harbor wave modeling. Melo and Guza (1991*a*; 1991*b*) made an early step to use it. They proposed a simplified model for wave propagation in the presence of rubble-mound jetties. Relying on the fact that waves approach the side walls at grazing angles, the model assumes the existence of a preferred direction of wave propagation and uses dissipative parabolic equations to describe the wave field. The jetties were represented simply as energy

dissipation regions. Two types of dissipation are considered: external (water motion over the sloping sides of the jetties) and internal (flow motion within the permeable core of the structure). Melo and Guza (1991*a*; 1991*b*) used the Lorenz principle to describe the dissipation equations. To solve the model equations, they resorted to the parabolic approximation (Melo and Guza (1991*a*; 1991*b*)). In this approach, the initial potential at the first row is given and then used as first estimate for the nonlinear terms in the equation. After that, the nonlinear term is used with the parabolic equation to compute the potential on the second row in an iterative fashion. Then, the solution obtained from the second row is then applied to the third row. This process is repeated until the solution of the last row is obtained. Although this approach (parabolic model) is easy to use, it does have limitations, such as no reflections and propagation largely along one axis. For this reason, the nonlinearity can be treated easily.

Another disadvantage is that multiple models may have to be used for complex geometries, which is inconvenient. For instance, in the study of the Mission Bay entrance channel, Melo and Gobbi (1998) used two parabolic approximation models. One model was for the straight channel with Cartesian coordinates and the other one based on polar coordinates was for the curved channel. The output of the “straight” model was an input for the “curved” model. One fact that should be noted is that this approach is based on an assumption that back-reflected wave field at the junction is negligible.

More recently, Sulisz (2005) developed a model based on the solution of the three-dimensional Laplace equation. Boundary conditions near the rubble-mound jetty

were described by the porosity and appropriate damping coefficients. In his study of the damping of wave propagation, he emphasized the effect of the geometry of the porous cave and the properties of the porous material which contributed to his final result. Initially, the model domain (channel and caves) was divided into several sub-domains. Then, each sub-domain was matched at the interfaces while using boundary-element method to solve the Laplace equation. Although Sulisz model (3D model) has no problem solving for the reflected and scattered waves in all directions, this approach has to be limited to small regions because it leads to large, full matrices.

Scope of Present Work

Currently, the elliptic mild-slope wave model is applied to perform simulations on the entire harbor domain. As I mentioned, two methods described above (i.e. the parabolic approximation model and the three-dimensional Laplace equation model) can only be used to selected portions of the overall domain. Aided by advances in iterative solution methods, in finite element grid generators, and in graphical user interfaces, robust codes are now available that can be efficiently applied to large domains of complex shape. See Panchang and Demirbilek (2001) for a review. The objective of my thesis is to explore the incorporation of the dissipative effects of rubble-mound jetties in elliptic models, thus extending capabilities of the models for practical engineering applications.

CHAPTER II

PERFORMANCE OF ELLIPTIC MODEL IN INLET

Many coastal projects include inlets, but few elliptic model simulations of inlets are available. Here, some analytical studies of inlets are used to test the performance of elliptic models. The analytical results of Dalrymple and Martin (2000) are used for comparison. Dalrymple and Martin (2000) also provide a simple suggestion for modeling dissipation in inlets, which is examined here.

In the following, the elliptic model is tested against the solution obtained by analytical model for three cases. The first and second tests consist of wave propagation in a rectangular channel with its full-reflecting side walls. The other walls AB, CD, EF and GH are fully reflected in all tests. The channel connects with the ocean and the bay, its length= l , width= $2b$. The schematic diagram of inlet in the tests is shown in Fig.3.

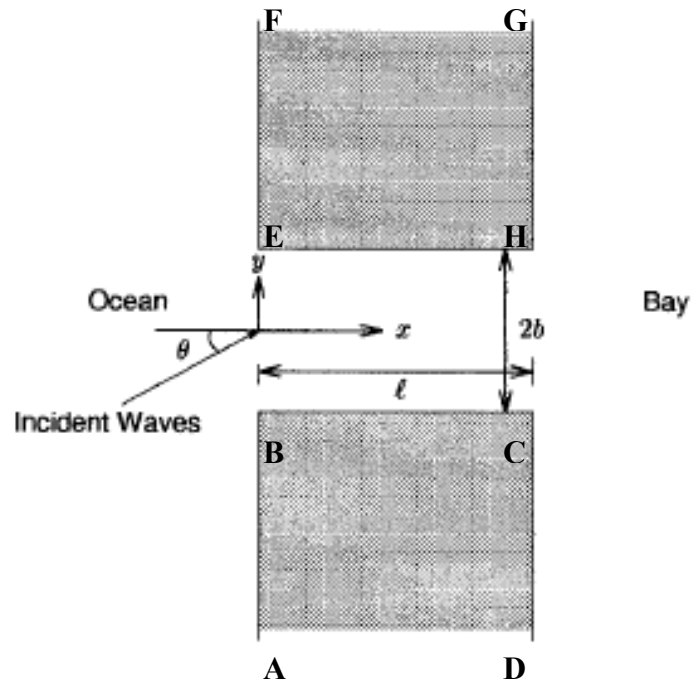


Fig. 3. Schematic diagram of inlet

For our domain, $l = 500$ m, $2b = 200$ m, and depth = 8 m, incident period = 12 s, and wavelength = 104.7 m. A semicircular external area connecting the channel has a radius of 600 m and the model domain contained 92,030 triangular elements and 46,608 nodes. The elliptic model solutions are compared with the results of Dalrymple and Martin (2000) in Figs. 4 and 5 for incidence wave angle = 0° and 45° . There are no major discrepancies between the results from these two models.

The third test consists of wave propagation in a rectangular channel connected to the ocean and bay with its partly-reflecting side walls. In this test, wave energy is partly absorbed by the side walls (reflection coefficient = 0.82 was used corresponding to a damping factor $\gamma = 1 \text{ m}^{-1}$ used by Dalrymple and Martin (2000)). The rectangular channel in the elliptic model domain is 1000 m long, 200 m wide and 8 m deep, which is connected to a semicircular external area with the radius 600 m. The model domain contained 67,250 triangular elements and 34,218 nodes. The elliptic model solutions are compared with the results of Dalrymple and Martin (2000) in Figs. 6 and 7 for incidence wave angle = 0° . The solutions produced nearly identical results.

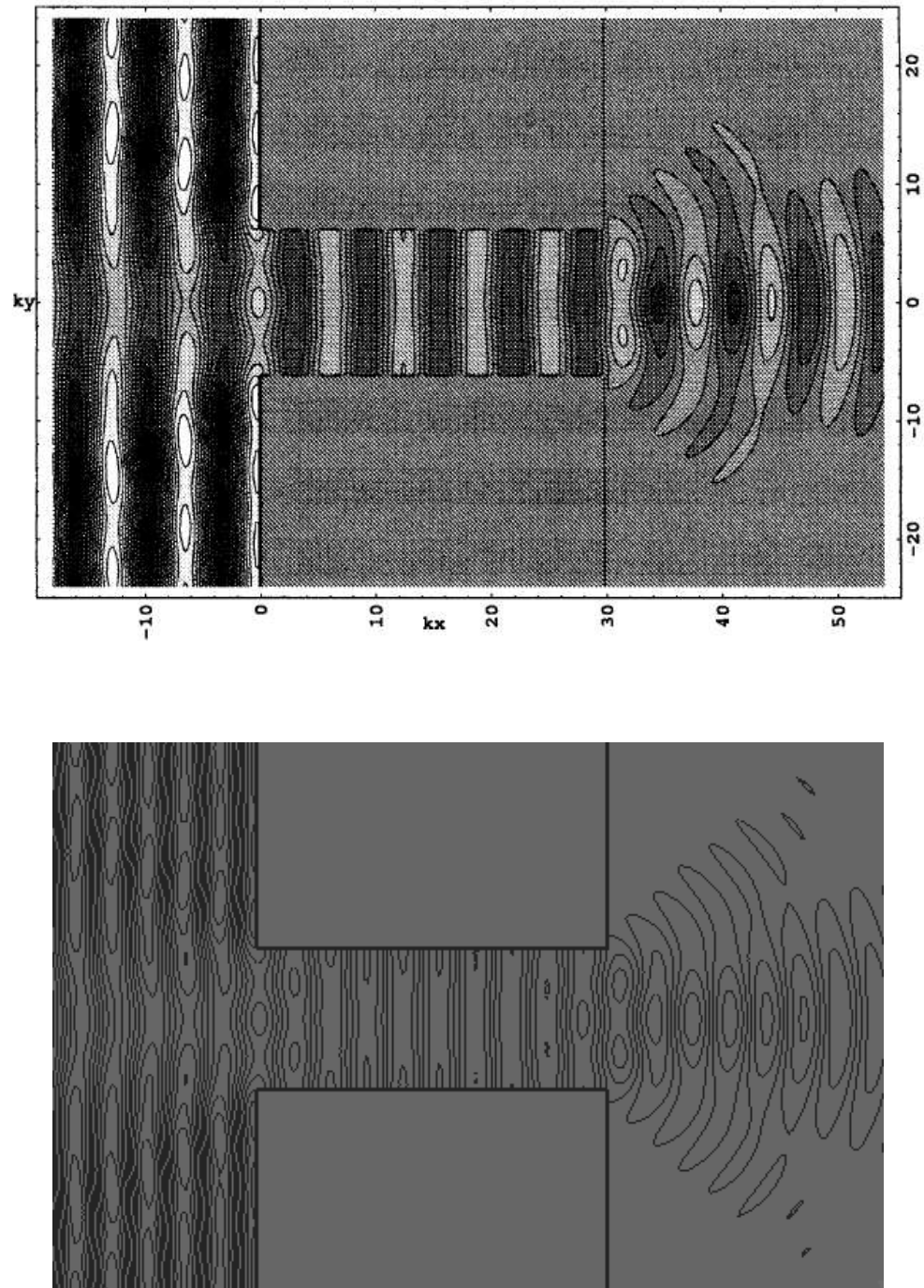


Fig. 4. Wave train normally incident to inlet; $kb = 6$, $kl = 30$ (Top: analytical method (Dalrymple and Martin 2000); bottom: present elliptic model)

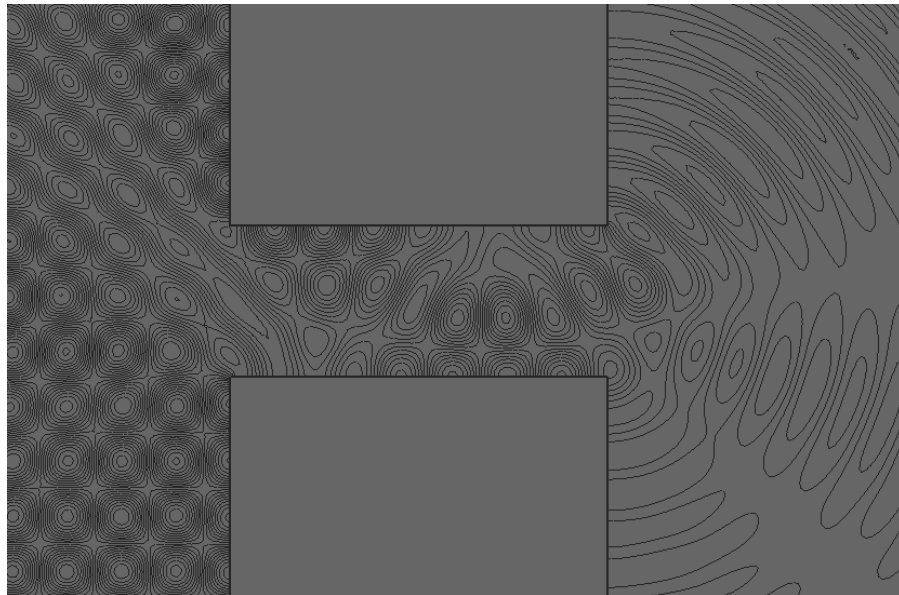
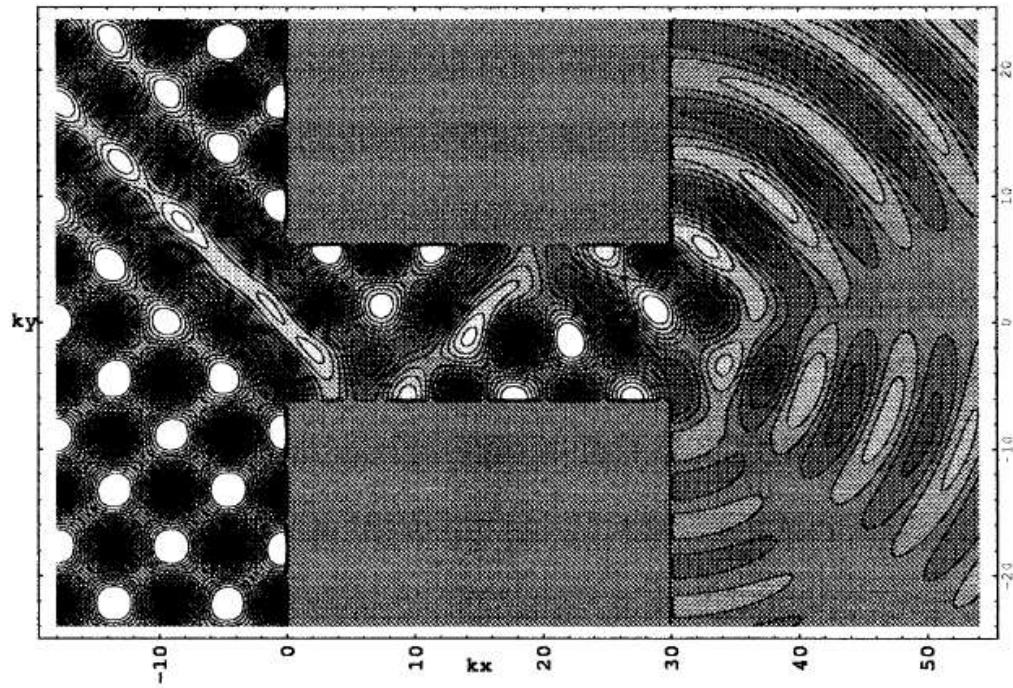


Fig. 5. Wave train incident at 45° to inlet; $kb = 6$, $kl = 30$ (Top: analytical method (Dalrymple and Martin 2000); bottom: present elliptic model)

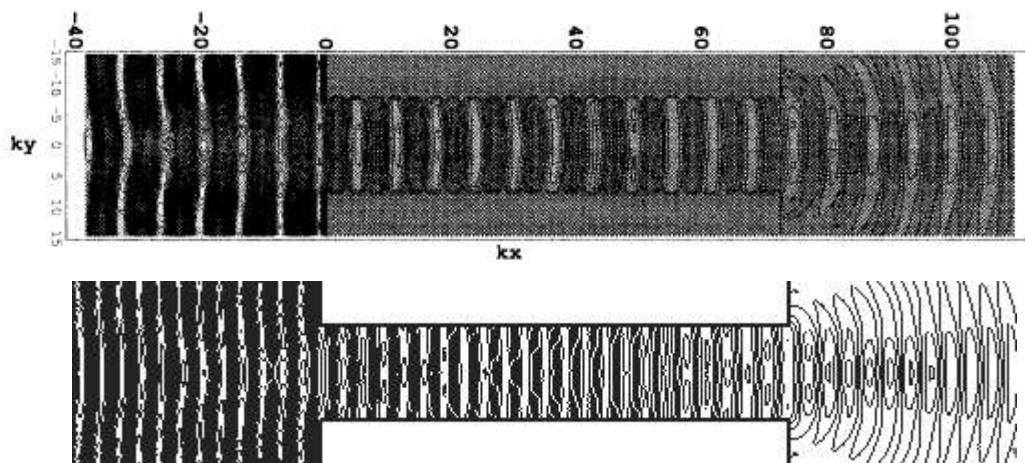


Fig. 6. Plane view of instantaneous water surface elevation in rectangular channel; ocean at left, bay at right (Top: analytical method (Dalrymple and Martin 2000); bottom: present elliptic model)

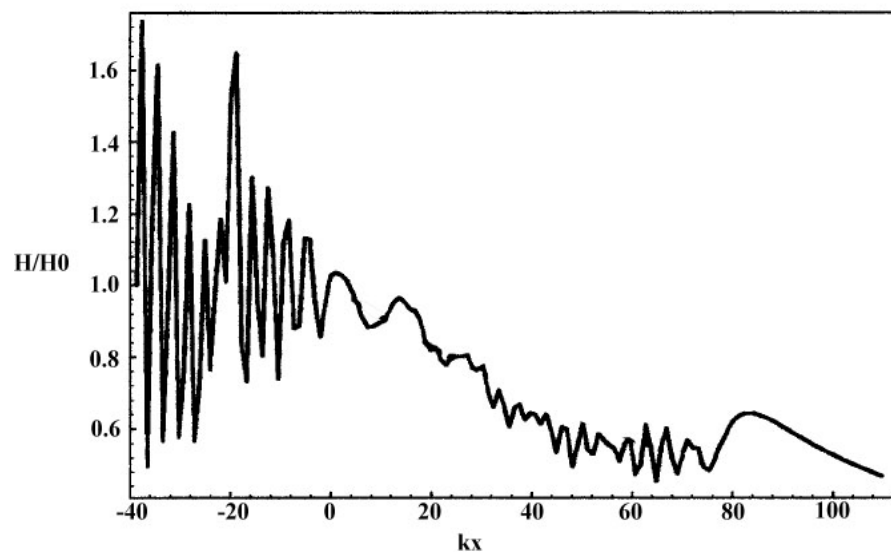


Fig. 7a. Decay of wave height along channel centerline; $\gamma=1 \text{ m}^{-1}$, $kb=7.32$, $kl=73.2$ (Analytical method (Dalrymple and Martin 2000))

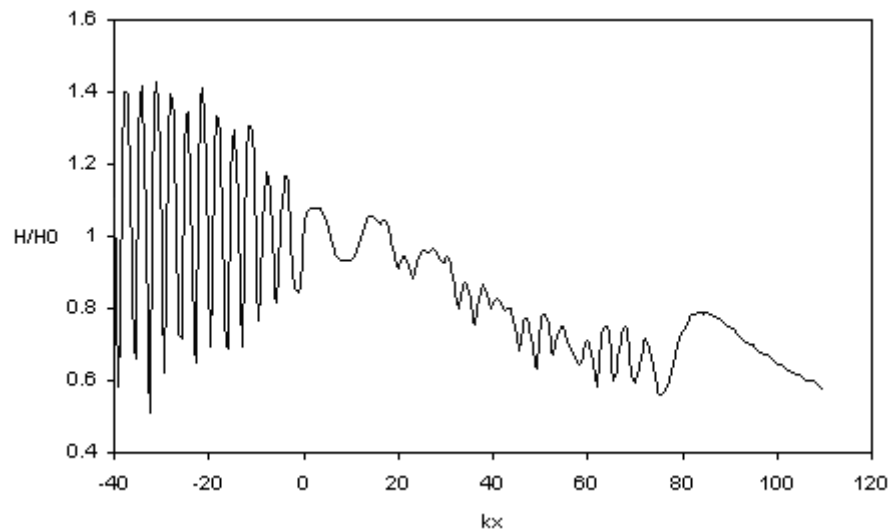


Fig. 7b. Decay of wave height along channel centerline; $\gamma=1 \text{ m}^{-1}$, $kb=7.32$, $kl= 73.2$
(Present elliptic model)

For these tests, analytical results of Dalrymple and Martin (2000) have been used above for validation of the elliptic model. Those results showed the elliptic model worked well for three tests. From the third test, it seems wave energy was absorbed in part by the side wall and the reflection coefficients may be used to simulate wave dissipation in the channel. This idea was suggested by Dalrymple and Martin (2000), who compared their solution qualitatively to those obtained by Melo and Guza (1991a; 1991b) for a case with rubble mound on the sides. Therefore, this idea was tested. The elliptic model was tested for wave dissipation in the straight channel and curved channel studied using parabolic approximation method by Melo and Guza (1991a; 1991b) and Melo and Gobi (1998). Comparisons of the results are shown in Figs. 8 and 9. The solutions show some qualitative similarity of two methods in these cases. However,

there is a quantitative discrepancy in the results of the two methods. Therefore, using the reflection coefficients to produce the dissipation effect may work well for solving some but not all cases. In the following part of this thesis, a more comprehensive approach of including wave dissipation in elliptic model will be introduced.

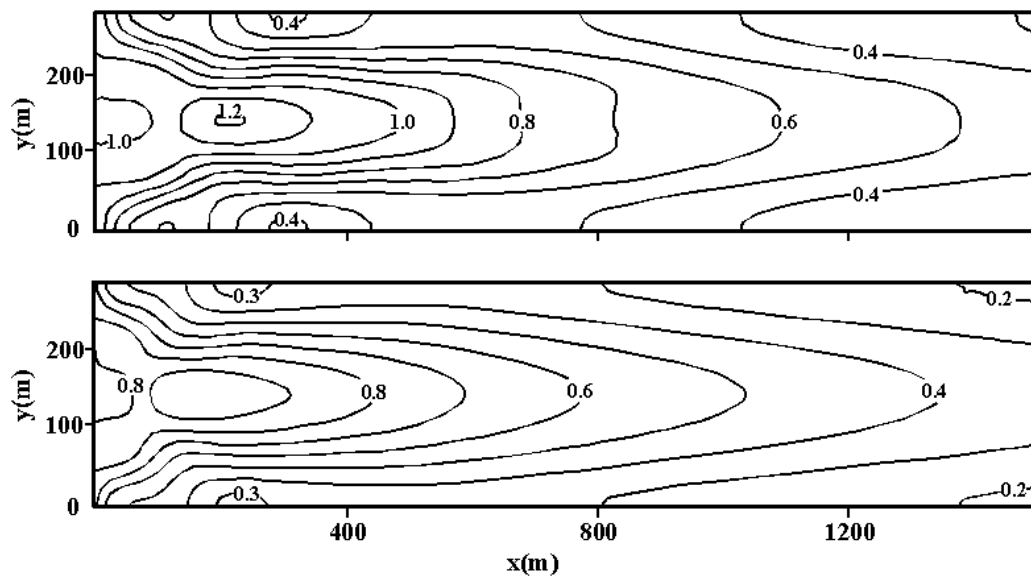


Fig. 8. Wave height comparison in the straight channel with dissipation for normally incident wave, reflection coefficient=0.55 (Top: parabolic approximation (Melo and Guza 1991a); bottom: elliptic model incorporating the reflection coefficients) (Reprinted with permission from ASCE.)

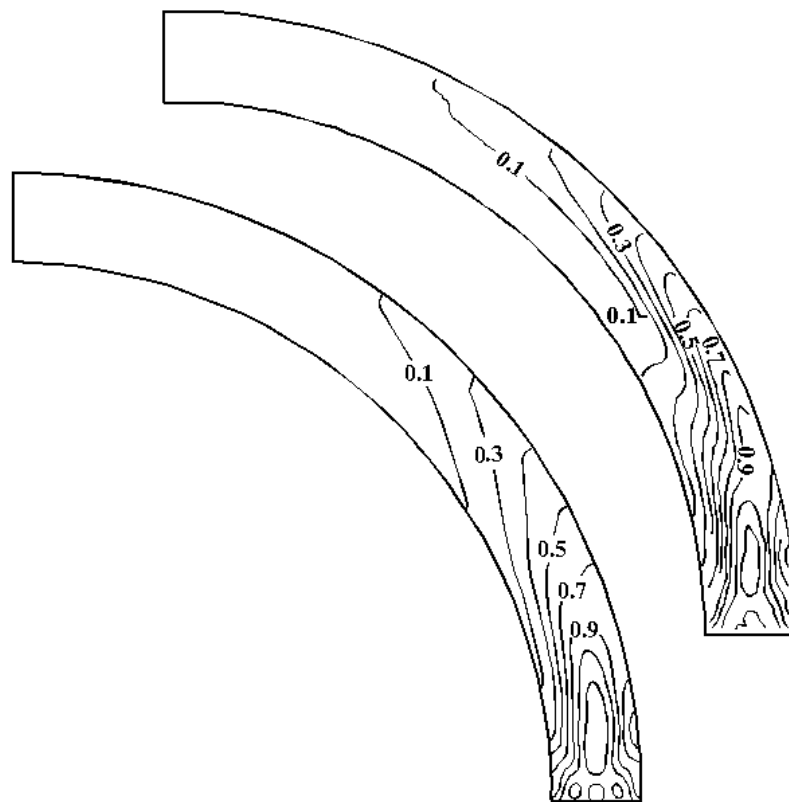


Fig. 9. Wave height comparison in narrow circular channel, with dissipation for normally incident wave, reflection coefficient=0.4 (Top: parabolic approximation (Melo and Gobbi 1998); bottom: elliptic model incorporating reflection coefficients) (Reprinted with permission from ASCE.)

CHAPTER III

METHODOLOGY

Mathematical Background

The governing equation for mild-slope wave model is:

$$\nabla \cdot (CC_g \nabla \phi) + (CC_g k^2) \phi = 0 \quad (1)$$

In equation (1), $\phi(x, y) = \phi_1 + i\phi_2$ = complex surface elevation function, from which the wave height can be obtained; $C(x, y)$ = phase velocity; $C_g(x, y)$ = group velocity; $k(x, y)$ = wave-number, related to the local depth $h(x, y)$ through the wave dispersion relation. Equation (1) is a two-dimensional, vertically-integrated form of the time-harmonic complex Laplace equation

$$\nabla^2 \Phi(x, y, z) = 0 \quad (2)$$

where

$$\Phi(x, y, z) = f(z)\Phi(x, y) \text{ and } f(z) = \cosh k(z + h) / \cosh(kh) \quad (3)$$

The vertical integrated form (1), together with the assumption (3), has been demonstrated to be valid for $|\nabla h| / kh \ll 1$ (Berkhoff 1976). This criterion is usually met in most applications. The elliptic equation (1) represents a boundary-value problem, and can have internal depth variations and boundaries. It is therefore widely used for performing wave simulations in regions with arbitrarily-shaped boundaries and arbitrary

depth variations. Unlike the parabolic approximation which has limitations on the angle of wave incidence or the degree and direction of wave reflection and scattering, equation (1) is more general.

In this thesis, one method is explored to solve the elliptic mild-slope equation, while simultaneously addressing the effects of rubble-mound jetties. Several investigators (e.g. Booij 1981; Dalrymple et al. 1984; Tsay et al. 1989) have proposed that frictional effects can be introduced in the mild-slope equation (1) by using a parameterized dissipation term as follows:

$$\nabla \cdot (CC_g \nabla \phi) + (CC_g k^2 + i\sigma w) \phi = 0 \quad (4)$$

where $\phi(x, y) = \phi_1 + i\phi_2 =$ complex surface elevation function, from which the wave height can be obtained; $i = \sqrt{-1}$; $\sigma =$ wave frequency under consideration; $w =$ friction factor.

Mathematical Formulation for Dissipation

One study of the wave dissipation was made by Dalrymple et al. (1984) and Tsay et al. (1989). They summarized several parameterized forms for the friction factor w . Some examples are:

1. Porous bottom:

$$k_i = \left(\frac{k\sigma}{\nu h} \right) \left(\frac{2kh}{2kh + \sinh 2kh} \right) \quad (5)$$

in which σ = wave frequency under consideration, ν = viscosity for water, k = wave number, h = water depth;

2. Viscous mud bottom of thickness d , viscosity ν_m , and density ρ_m :

$$k_i = \frac{(2d)^{-2} \frac{gk}{\sigma^2} \left(\frac{\nu}{\sigma}\right)^{1/2} \left\{ \left[k(d+h) - \frac{\sigma^2}{gk} \right]^2 + \left[1 + \left(\frac{\rho_m}{\rho}\right) \left(\frac{\nu_m}{\nu}\right)^{1/2} \right] \left[\left(\frac{\sigma^2}{gk}\right) - kh \right]^2 \right\}}{\left[1 + \left(\frac{\rho}{\rho_m}\right) \left(\frac{\nu}{\nu_m}\right)^{1/2} \right] \left[1 + \left(\frac{\rho_m}{\rho} - 1\right) \left(1 - \frac{gk}{\sigma^2} kh\right)^2 \right]} \quad (6)$$

in which k_i is the shallow water wave number (for simplicity).

3. Laminar bottom boundary layer:

$$k_i = \frac{k^2 \sqrt{\frac{\nu}{2\sigma}}}{n \sinh 2kh} \quad (7)$$

4. Densely packed surface film:

$$k_i = \frac{k^2 \sqrt{\frac{\nu}{2\sigma}}}{2\pi \tanh 2kh} \quad (8)$$

5. Natural vegetation (seaweed, trees, etc.)

$$\alpha = \frac{2C_D}{3\pi} \left(\frac{D}{b}\right) \left(\frac{a_0}{b}\right) \left[\sinh^3 ks + 3 \sinh ks \right] \left[\frac{4k}{3 \sinh kh (\sinh 2kh + 2kh)} \right] \quad (9)$$

in which α is a damping factor, a_0 is the initial wave amplitude, s is height above bottom, b is spacing of cylinders or plants, D is diameter of cylinders or plants, and C_D is the representative drag coefficient. For the numerical modeling it is often sufficient, for small grid sizes,

$$w = \begin{pmatrix} \frac{2n\sigma k_i}{k} \\ \frac{k}{2n\sigma\alpha} \\ k \end{pmatrix} \text{ for } (k_i, \alpha) \ll k. \quad (10)$$

The governing equation can be solved with w specified and boundary conditions given. However, the solution of the elliptic equation for a large area and irregular bathymetry on damping would require a large finite element or finite difference model. Dalrymple et al (1984) found a way to use the parabolic form of the governing equation to reduce the computational effort and time. But, this method is not as suitable to the full solution for many domains. Moreover, their formulations do not appear to be directly applicable to the dissipative effects of rubble-mound jetties.

However, Melo and Guza (1991a) found a different way to study the wave dissipation. They employed a parameterization based on the Lorentz principle. In their study, the jetty cross-section was recommended to be divided into two areas: external and internal areas. The submerged portion of the jetty is described as an external dissipation region, and the part further away from the water is described as an internal dissipation region (Fig. 10).

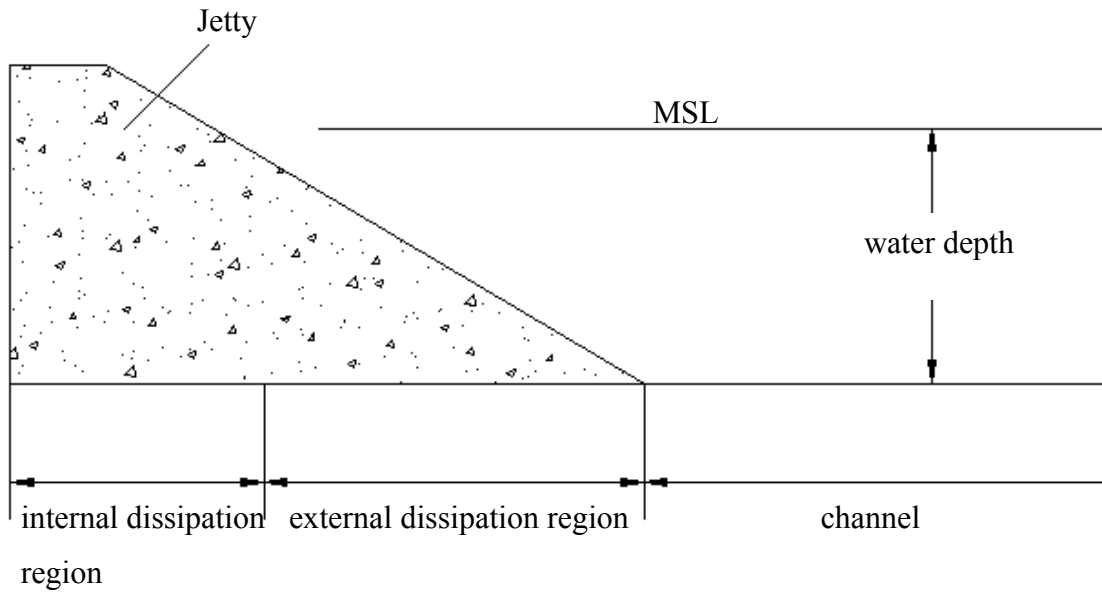


Fig. 10. Definition sketch for jetty modeling

Two parameters, f_{ext} and f_{int} , are referred to as the dissipation coefficients assigned to each region. Both dissipation coefficients may be related to the original friction factor w as follows:

$$w = f k C_g, \text{ where } f = f_{int} \text{ or } f_{ext} \quad (11)$$

The external dissipation coefficient f_{ext} depends on the wave energy dissipated per unit area over a rough, steep slope. Since this is difficult to estimate, Melo and Guza (1991a) have related it to a local reflection coefficient (R) in a simple manner:

$$f_{ext} = \frac{1 - R^2}{k D_e} \quad (12)$$

where D_e = width of the external dissipation region of the model jetty. When R is specified by the user, f_{ext} is easy to estimate. On the other hand, the internal dissipation

f_{int} is more complicated to estimate. Melo & Guza (1991a) and Sulisz (2005) formulated the dissipation in the pores as a combination of laminar and turbulent stresses ($= \alpha q + \beta |q|q$, where q represents flux). Then they used the Lorentz principle of equivalent work to relate f_{int} to α and β :

$$f_{int} = \frac{1}{\sigma} (\alpha + \beta \lambda_q) \quad (13)$$

In (12), λ_q is a function of the velocity through an elemental porous volume V , estimated by Melo & Guza (1990) as:

$$\lambda_q = \frac{8}{3\pi} q^*(x) \quad (14)$$

where q^* is the amplitude of a representative mean seepage velocity within V , given by

$$q^*(x) = \frac{1}{D_c X_c} \int_{D_c} \int_{X_c} \left| \frac{-ig}{\sigma(S - if_{int})} \right| |\nabla \phi(x, y)| dx dy \quad (15)$$

where D_c is small core width, X_c is a suitably small length of core. In accordance with the level of approximation used herein, (15) can be further reduced to,

$$q^*(x) = \left| \frac{-igk}{\sigma(S - if_{int})} \right| |A^*(x)| \quad (16)$$

then,

$$\lambda_q = \frac{8}{3\pi} \left| \frac{-igk}{\sigma(S - if_{int})} \right| |A^*(x)| \quad (17)$$

where $|A^*(x)|$ is a characteristic mean wave amplitude within V . For the laminar and turbulent stress coefficients α and β , Melo and Guza (1991a) suggest the following descriptions:

$$\alpha = \alpha_0 \frac{(1-n)^3}{n} \frac{\nu}{d^2} \quad \beta = \beta_0 \frac{(1-n)}{n} \frac{1}{d} \quad (18)$$

where n is the porosity (ratio of void to total volume) for rubble-mound structures; ν is the kinematic viscosity of water; d is the rock diameter; and α_0 and β_0 are constants with average values of 1,000 and 2.7, respectively. Therefore, the resulting parameterization for f_{int} is a function of the wave properties and renders the model nonlinear. In this thesis, the dissipation theory of Melo and Guza (1991a; 1991b) is applied in the elliptic mild-slope equation.

Solution of the Mild-slope Equation with Dissipation

To obtain the solution of the mild-slope equation with dissipation, the friction factor w is needed to know. After w is computed, the solution of the elliptic equation (4) can be obtained for any domain of arbitrary shape (Tsay et al. 1989; Demirbilek and Panchang 1998). Boundary conditions along coastlines and other closed boundaries (Fig. 11) can be written in terms of the normal derivative and a user-specified reflection coefficient.

Open Boundary Conditions

Along the open boundary (denoted by the semicircle in Fig. 11), the potential ϕ consists of three components: the incident wave (ϕ_i) that must be specified to force the model, a reflected wave (ϕ_r) that would exist in the absence of the harbor, and a scattered wave (ϕ_s) that results as a consequence of the harbor. With appropriate descriptions for these components, a boundary condition can be developed along the semicircle. The procedure can be summarized as follows. The exterior region is represented by two one-dimensional transects denoted by AB and CD (with depths varying in the cross-shore direction only). The incident wave is specified at the offshore end. A one-dimensional version of equation (4) is used to solve for the combination of ϕ_i and ϕ_r (denoted by ϕ_o) along the transects.

$$\frac{d}{dx} \left(CC_g \frac{d\phi_o}{dx} \right) + Ck(C_g k + iw) \phi_o = 0 \quad (19)$$

This equation is solved by finite differences, with w specified as described later. The result ϕ_o is then laterally transposed on to the semicircle. For the scattered wave, the radiation condition is

$$\frac{\partial \phi_s}{\partial n} = \left(ik - \frac{1}{2r} \right) \phi_s \quad (20)$$

Introducing $\phi_s = \phi - \phi_o$ into equation (20) gives the appropriate radiation equation for the scattered wave and completes the treatment of the open boundary condition:

$$\frac{\partial \phi}{\partial n} = \frac{\partial \phi_0}{\partial n} + \left(ik - \frac{1}{2r}\right)(\phi - \phi_0) \quad (21)$$

Closed Boundary Conditions

Along the coastline and surface-protruding structures, the following boundary condition has traditionally been used (e.g. Berkhoff 1976; Tsay & Liu 1983; Tsay et al. 1989; Oliveira and Anastasiou 1998; Li 1994a):

$$\frac{\partial \phi}{\partial n} = ik \frac{1 - K_r}{1 + K_r} \phi \quad (22)$$

where n is the outward normal to the boundary, and the reflection coefficient K_r varies between 0 and 1.

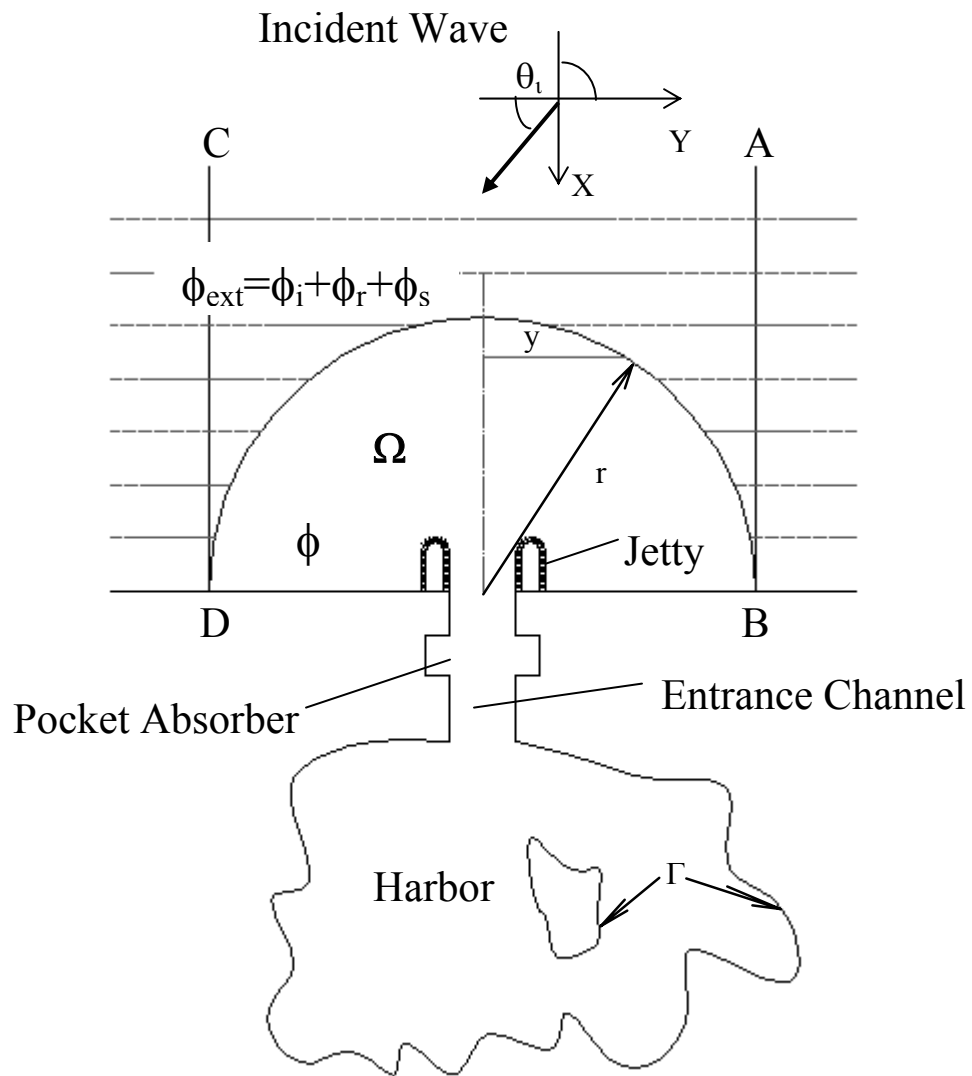


Fig. 11. Harbor wave model domain; definition sketch

Numerical Solution

The finite element method is used for a numerical solution (Demirbilek and Panchang 1998). A typical harbor model grid contains about 250,000 nodes (depending on the harbor dimensions and the desired resolution of $L/10$) and a solution can be obtained by the method of conjugate gradients (Li 1994; Panchang et al. 1991; see also Bova et al. 2000). The following section presents the detailed procedure first proposed by Panchang et al. (1991). After discretization, the governing equation (4) may be expressed in matrix form as

$$[A]\{\phi\} = \{f\} \quad (23)$$

where $[A]$ is the system matrix, $\{\phi\}$ is the unknown vector of the desired grid-point values of the wave potential, and $\{f\}$ is a vector that contains information from the discretized boundary conditions. One method to solve the above equation group is Gaussian elimination, which requires storage for the matrix $[A]$. Note that even when there are as few as 100 unknowns, $[A]$ contains 100×100 complex elements. Therefore computer storage can be one problem, and solution by direct Gaussian elimination is practically impossible for big domains. (In this study, the domain contains at least 10 wave lengths.)

As an alternative to Gaussian elimination, the resulting discretized system of linear equations can be solved by the method of Conjugate Gradients (CG, Panchang et al. 1991). This method does not require the storage of $[A]$, but it converges only when the

system matrix is symmetric and positive-definite. In order to use the conjugate gradient method, the matrix $[A]$ must be modified to be symmetric and positive-definite, or else the conjugate gradient method will not converge. A remedy (Panchang et al. 1991) is to use the Gauss transformation, i.e. multiply equation (23) by $[A^*]$, the complex conjugate transpose of $[A]$:

$$[A^*][A]\{\phi\} = [A^*]\{f\} \quad (24)$$

The new coefficient matrix $[A^*][A]$ is always symmetric and positive-definite, and the modified CG procedure for equation (24) will converge. The algorithm was proposed by Panchang et al. (1991) as follows:

1. Select trial values ϕ_0 (i.e. $i=0^{\text{th}}$ iteration) for all grid points where the solution is desired.
2. Compute for all points $r_0 = f - A\phi_0$ and $p_0 = A^* r_0$.
3. Compute for i^{th} iteration: $\alpha_i = \frac{|A^* r_i|^2}{|Ap_i|^2}$.
4. Update $\phi_{i+1} = \phi_i + \alpha_i p_i$.
5. Check for convergence of solution.
6. Compute, for each grid point, $r_{i+1} = r_i - \alpha_i Ap_i$.

7. Compute for i^{th} iteration: $\beta_i = \frac{|A * r_{i+1}|^2}{|A * r_i|^2}$.
8. Compute $p_{i+1} = A * r_{i+1} + \beta_i p_i$.
9. Set $i=i+1$, and go to step 3.

The above procedure is guaranteed convergence although the speed can be slow. This is because the transformed equation (24) is less efficient than the original equation (23).

Nonlinear Iteration

Since the dissipation factor w (or, more specifically, f_{int}) is a function of the wave amplitude (according to (11) and (12)) and is unknown, (4) must be solved by iteration. Each round of the solution for a specified w requires several thousand iterations and the overall process is time-intensive. For the first iteration, w is set equal to 0 (i.e. linear (frictionless) solutions are obtained). Thereafter, w is updated every nonlinear round using the resulting wave heights and (4) is solved again. The process is repeated until the solutions converge. In this thesis, the effect of incorporating the wave dissipating model into one simulation was examined. This simulation has been performed by Melo and Guza (1991a) (shown in Fig.19) in a straight channel, which will be described in a later chapter. The overall problem was assumed to have been solved when the maximum difference δ , at any grid point between two successive nonlinear solutions reaches 10^{-4} or less. Further, the maximum number of non-linear iterations was set to 15. To explore the behavior of the solution of this highly nonlinear problem, three locations ($x=0$; $x=600$; $x=1200$) inside the model domain were randomly selected to observe local wave

fields. Final results at selected locations are given in Fig 12. Obviously, the trends of wave heights were initially decreasing and converged after about 11 non-linear iterations with $\delta=5.17 \times 10^{-4}$. No unusual difficulties occurred during the iterations. Usually, successive rounds of nonlinear iterations took fewer CG iterations.

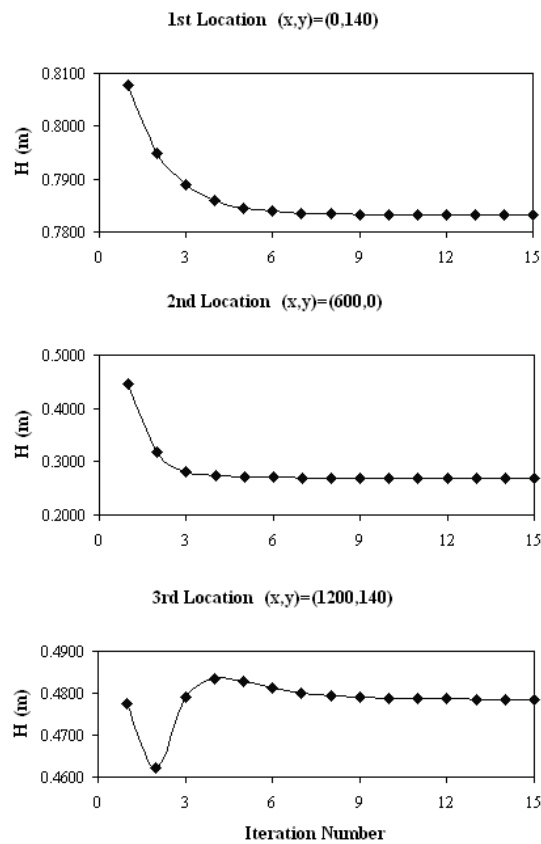


Fig. 12. Non-linear convergence of the elliptic model

CHAPTER IV

VALIDATION AGAINST OTHER MATHEMATICAL SOLUTIONS

Elementary Test

The model described above was first tested against solutions obtained by other methods. Two elementary cases, wave propagation over constant-depth regions with two friction values (Dalrymple et al. 1984), were simulated to test the code. In Fig. 13, the first case is shown with a region (610m*305m) of strong damping. Here w is fixed as 0.236 and the wave parameters for this and subsequent cases are a wave height of 6.1m, a wave period of 20 sec and a water depth of 15.2 m. The depicted region is a semi-circle area of radius 5000m represented by 80,345 nodes. The case of a larger region of damping (2930m*915m), with lesser values of w ($w=0.031$) is shown in Fig. 14. The plotted region is a semi-circle domain with a 6000m radius represented by 115,489 nodes. The effect of oblique incidence is shown in Fig. 15. The results of two cases obtained by the elliptic model match with those obtained by Dalrymple et al. (1984).

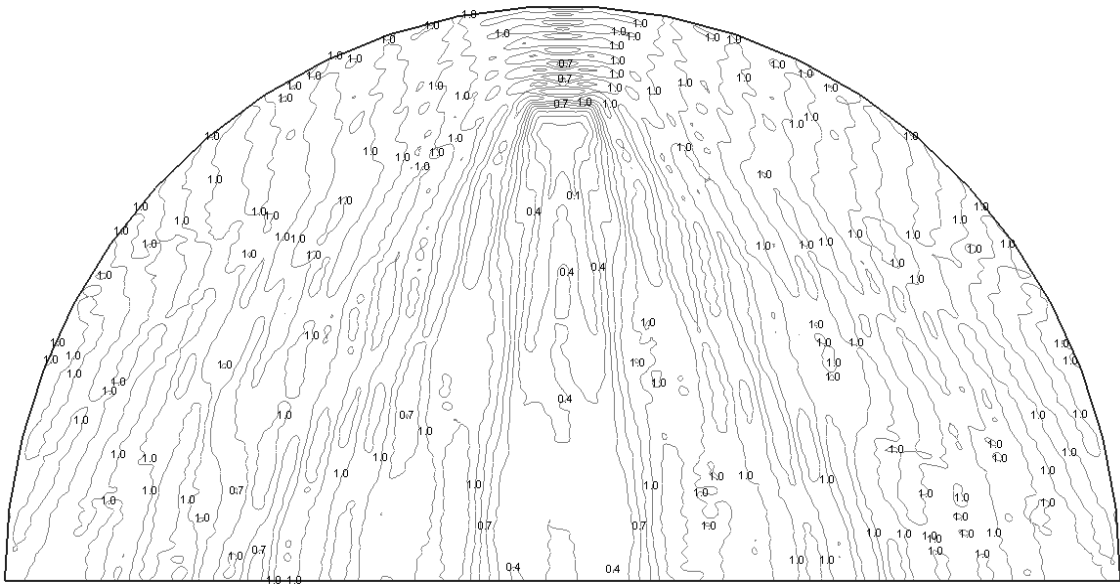


Fig. 13. Wave field in and around region of strong damping

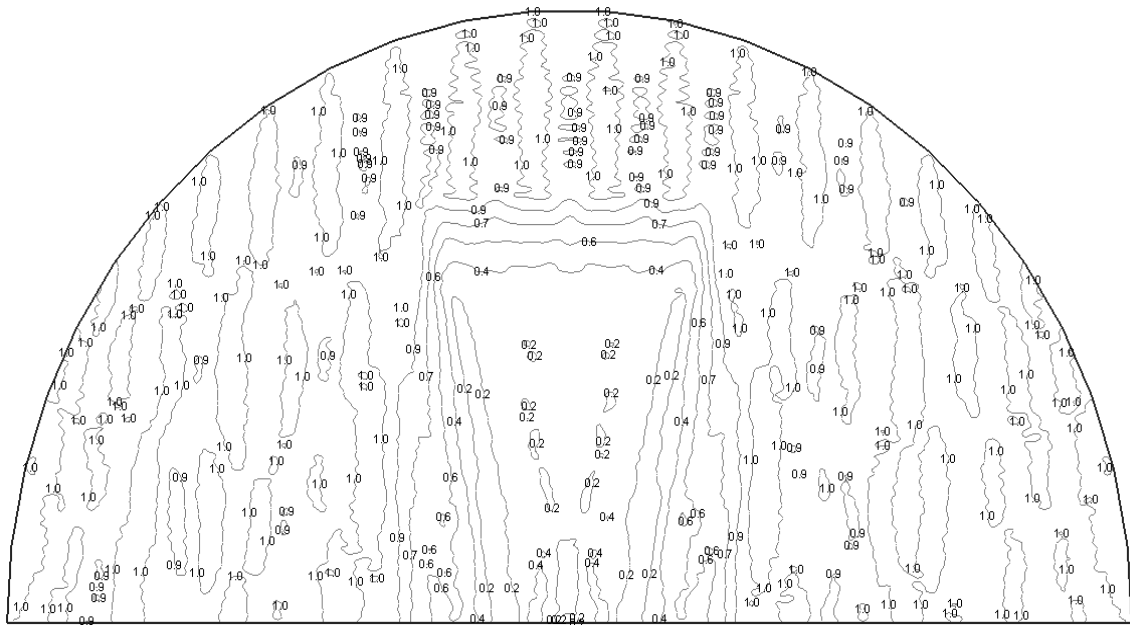


Fig. 14. Wave field in and around region of weaker damping

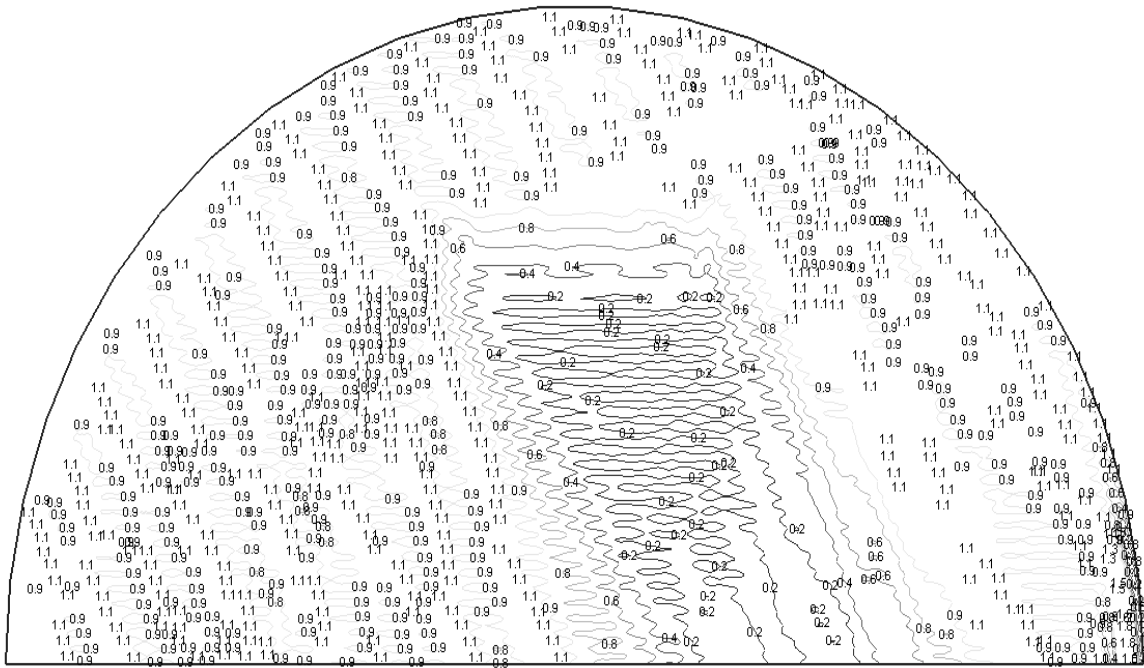


Fig. 15. Wave field in and around region of weaker damping and 30° angle of incidence

Pocket Wave Absorber

The first simulation shows wave propagation in a rectangular channel with two pocket wave absorbers (configuration D in Fig. 2). The geometry consists of a channel of depth 1 m and width 4 m. Two rectangular pocket absorbers of length 8 m (along the channel) and width 1 m are placed along the sides. An incident wave of amplitude 0.5 m and period 2.3 s was specified for the simulation. Rubble mound (stone) was placed in the pocket absorber and except this there are not any rubble-mound structures installed along the boundaries. Rubble mound was described by $f_{int} = 0.25$ and $f_{ext} = 0$. The non-rubble-mound boundaries were treated as fully reflective. The solution of the elliptic equation (4) is compared in Fig. 16b to that obtained by Sulisz (2005) using the 3-

dimensional Laplace equation in Fig. 16a. Figs. 16a and 16b show only half the domain for reasons of symmetry. The results are largely the same. Both solutions show increased wave heights on the up-wave side of the pocket wave absorbers and smaller wave on the down-wave side. Fig. 17 shows modeled wave heights (the elliptic model) along three transects and reflections on the up-wave side can be as high as 40%.

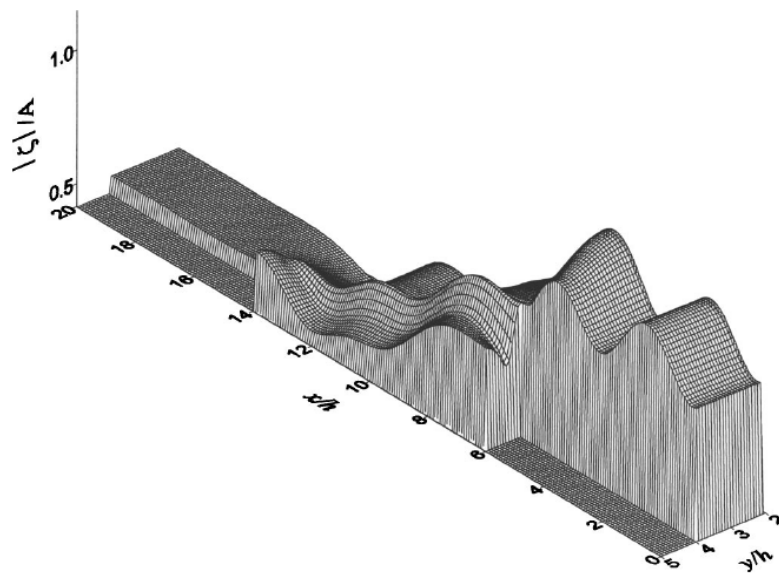


Fig. 16a. Wave amplitude comparison in a channel with two pocket wave absorbers (3D model (Sulisz 2005)) (Reprinted with permission from ASCE.)

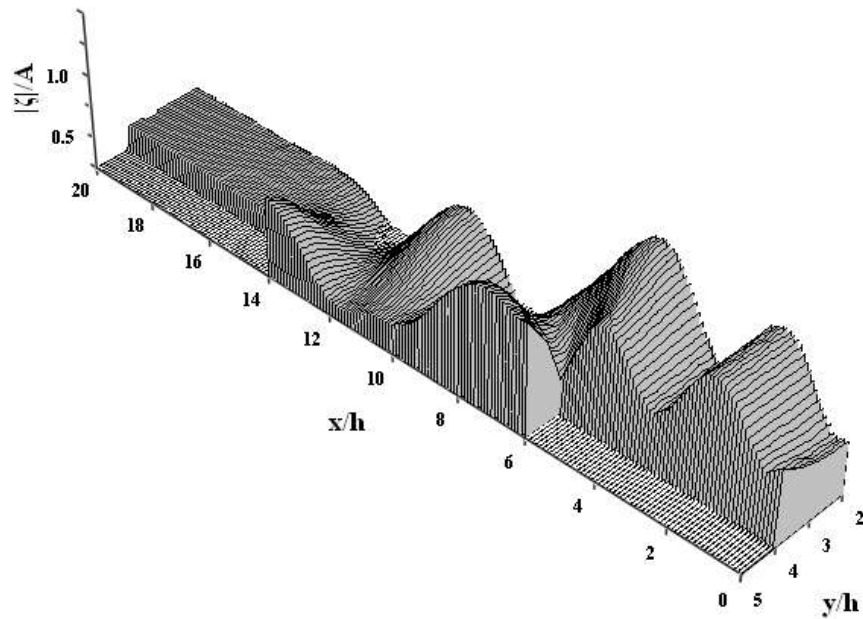


Fig. 16b. Wave amplitude comparison in a channel with two pocket wave absorbers
(present elliptic model)

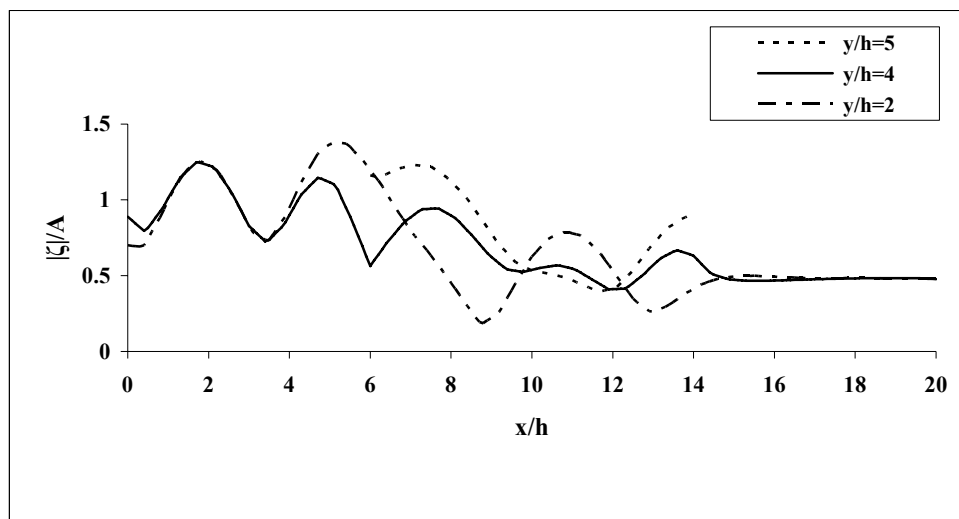


Fig. 17. Modeled (normalized) wave amplitudes

Straight Channel Bounded by Rubble Mound Jetties

The second simulation consists of wave propagation in a straight channel bounded laterally by rubble mound jetties (Fig. 18). The jetty parameters are $n = 0.45$; $d = 1.25$ m; and $f_{ext} = 0.5$. And the input wave has amplitude of 0.4 m and period 14 s. A solution to this problem has been previously obtained by Melo and Guza (1991a). They were using parabolic approximations accurate to different orders. The elliptic equation model domain used here consisted of the rectangular region and a semicircular open boundary. The semicircular external area is of radius 1140 m and contained 97,761 triangular elements. The solution converged to a (normalized) tolerance of the order of 10^{-6} after about 19 iterations. The elliptic model solutions are compared against the results of Melo and Guza (1991a) in Figs. 19 and 20 for incident wave angles = 0° and 10° . The discrepancies between the two sets of results are small.

Generally, the 3D Laplace model is a more complete model and the 2D parabolic method is an approximation of the elliptic model. Comparing these two solutions with the present (2d elliptic model) solution, the similarity suggests the present model is reliable. In the following section, therefore, we explore additional cases with the present and develop solutions to them.

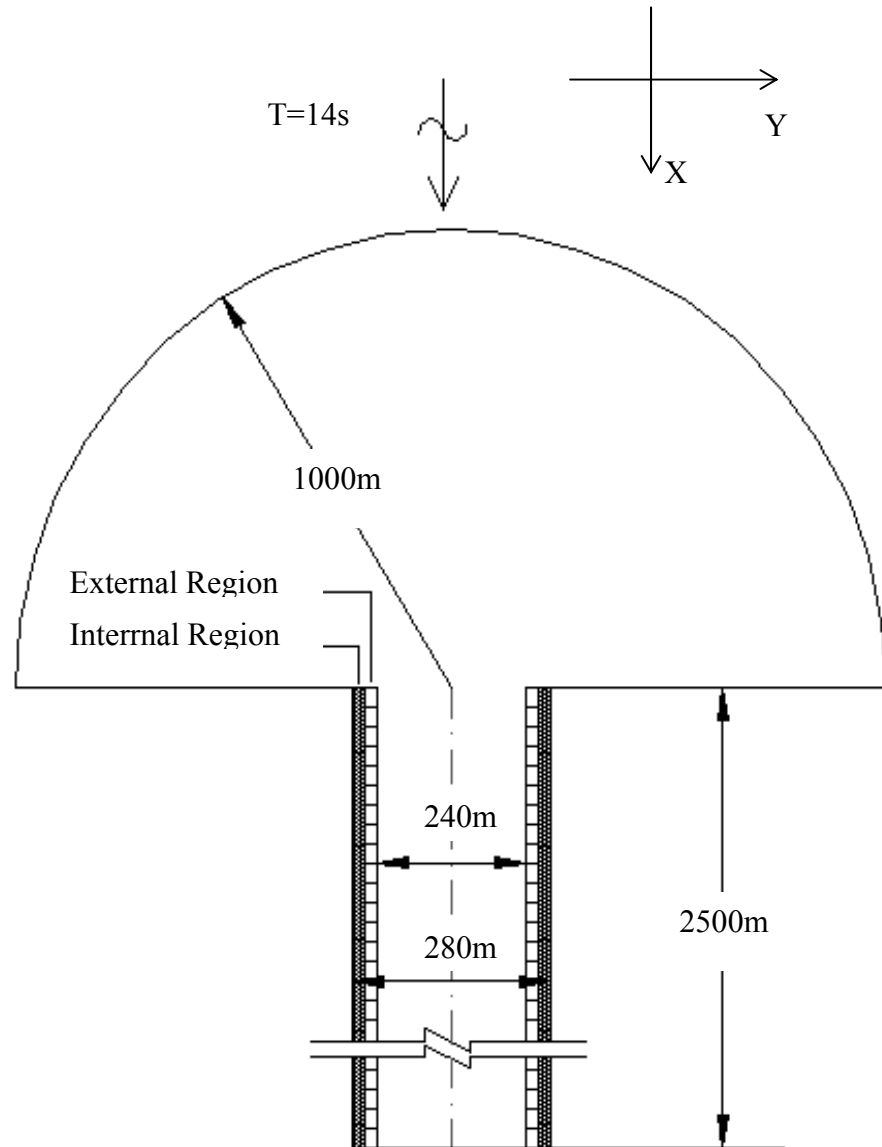


Fig. 18. Straight channel model domain (after Melo and Guza 1991a)

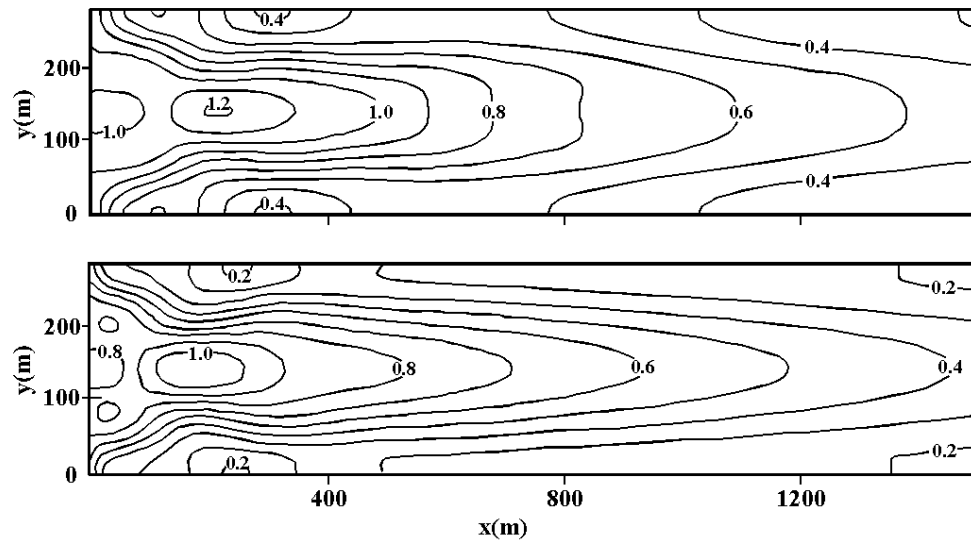


Fig. 19. Wave height comparison for $\theta=0^\circ$. (Top: parabolic approximation (Melo and Guza 1991a); bottom: present elliptic model) (Reprinted with permission from ASCE.)

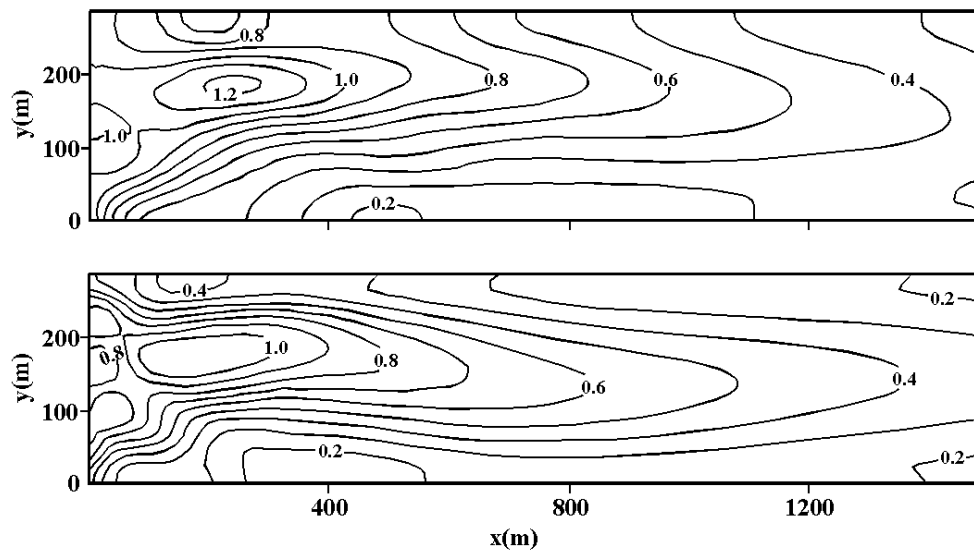


Fig. 20. Wave height comparison for $\theta=10^\circ$. (Top: parabolic approximation (Melo and Guza 1991a); bottom: present elliptic model) (Reprinted with permission from ASCE.)

Other Simulations

We first consider the case of wave propagation in circular (or curved) channels with jettied side walls. Solutions to this problem have been obtained by Melo and Gobbi (1998). They used a parabolic approximation in polar coordinates by way of an extension of the straight channel case described above. Two cases with different radii of curvature were examined. To study the effects of the jetty wall on the solutions, they performed simulations with and without the stone rubble along the walls (i.e. with and without w). The results from the present elliptic model are compared with results of Melo and Gobbi (1998) in Figures 21 - 24. Figs 21 & 22 (the no-friction case) show that results of the parabolic approximation are similar to the full elliptic model solution. The limitation of the parabolic model lies in the direction of wave scattering, which makes the solution inaccurate in some special cases. However, the similarity of two solutions is somewhat surprising. On the other hand, when the dissipative effects of the jetties are introduced the differences become much greater (Figs. 23 & 24). The wave height contours resulting from the elliptic model appear to be shifted towards the inside of the curve relative to those resulting from the parabolic model. Since the parabolic approximation can accommodate wave scattering in a limited aperture, one can infer that the enhanced wave scattering induced by the jetties is an impediment to the approximate model. But the elliptic model has no such restrictions. Therefore, the results shown in Fig. 24 may be used as the benchmark solutions for future modeling studies.

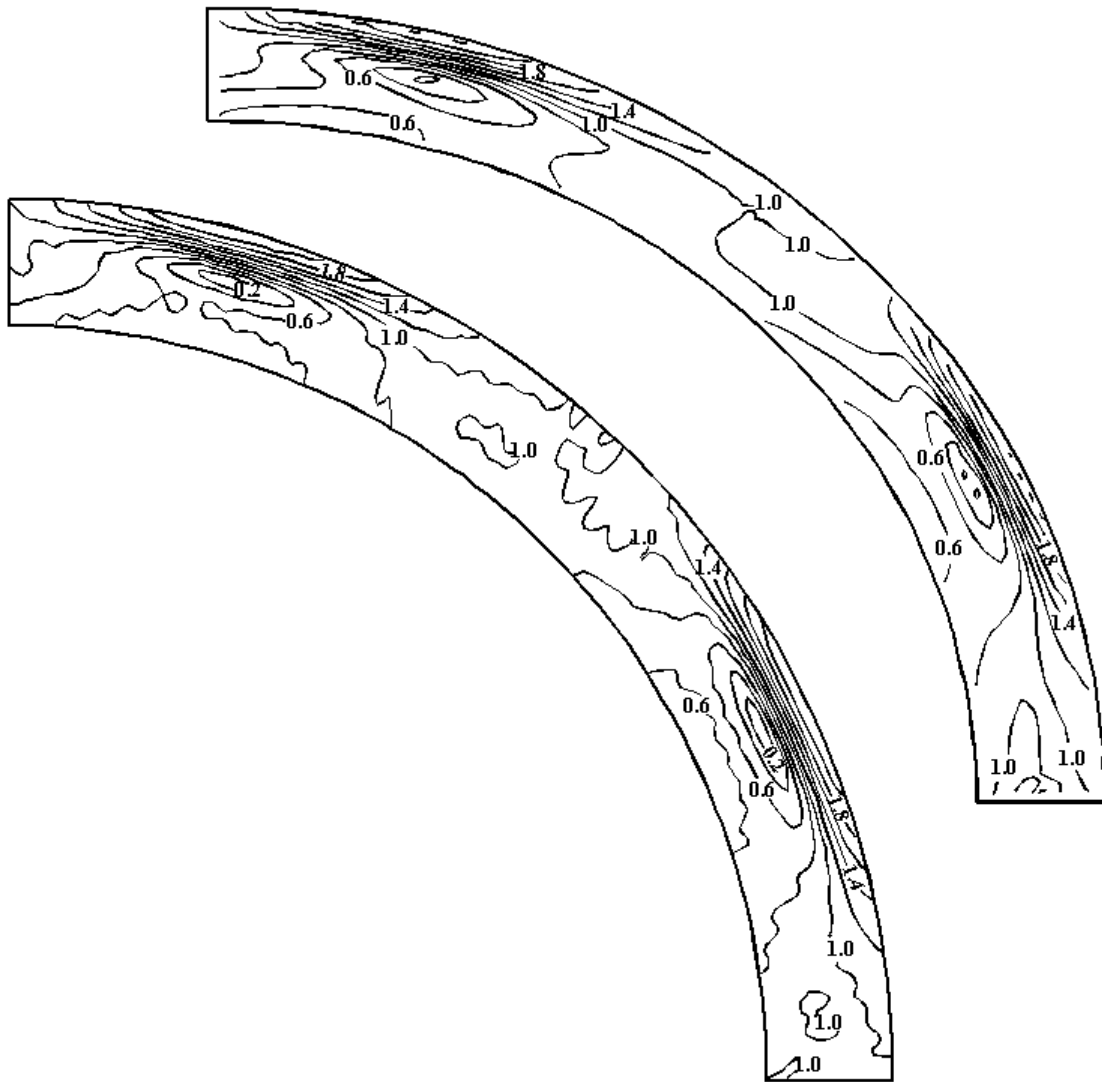


Fig. 21. Wave height comparison in narrow circular channel, no dissipation. (Top: parabolic approximation (Melo and Gobbi 1998); bottom: present elliptic model)

(Reprinted with permission from ASCE.)

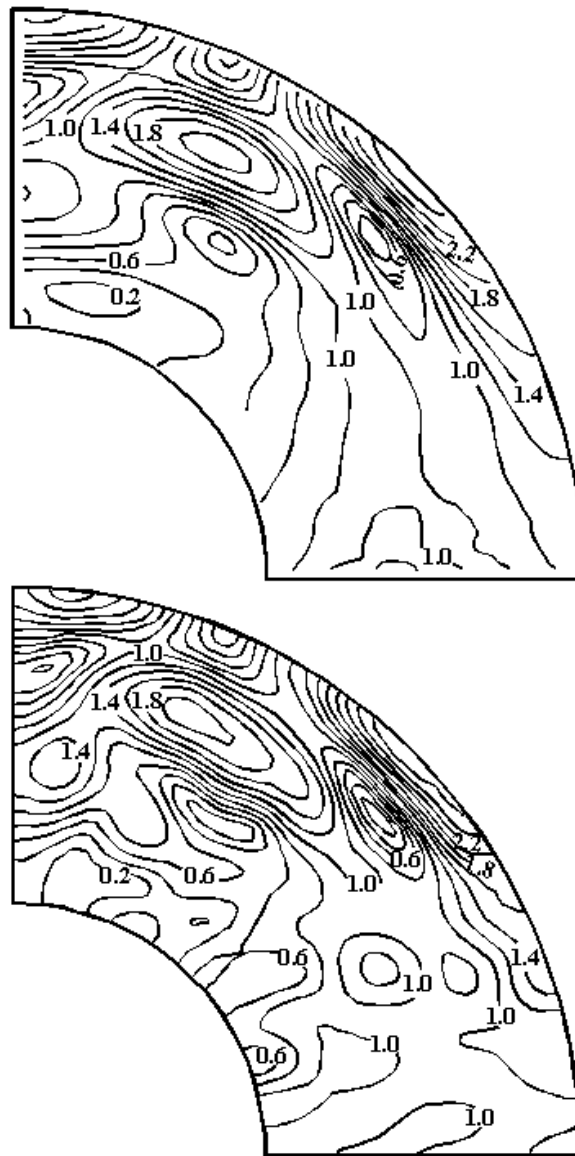


Fig. 22. Wave height comparison in wide circular channel, no dissipation. (Top: parabolic approximation (Melo and Gobbi 1998); bottom: present elliptic model) (Reprinted with permission from ASCE.)

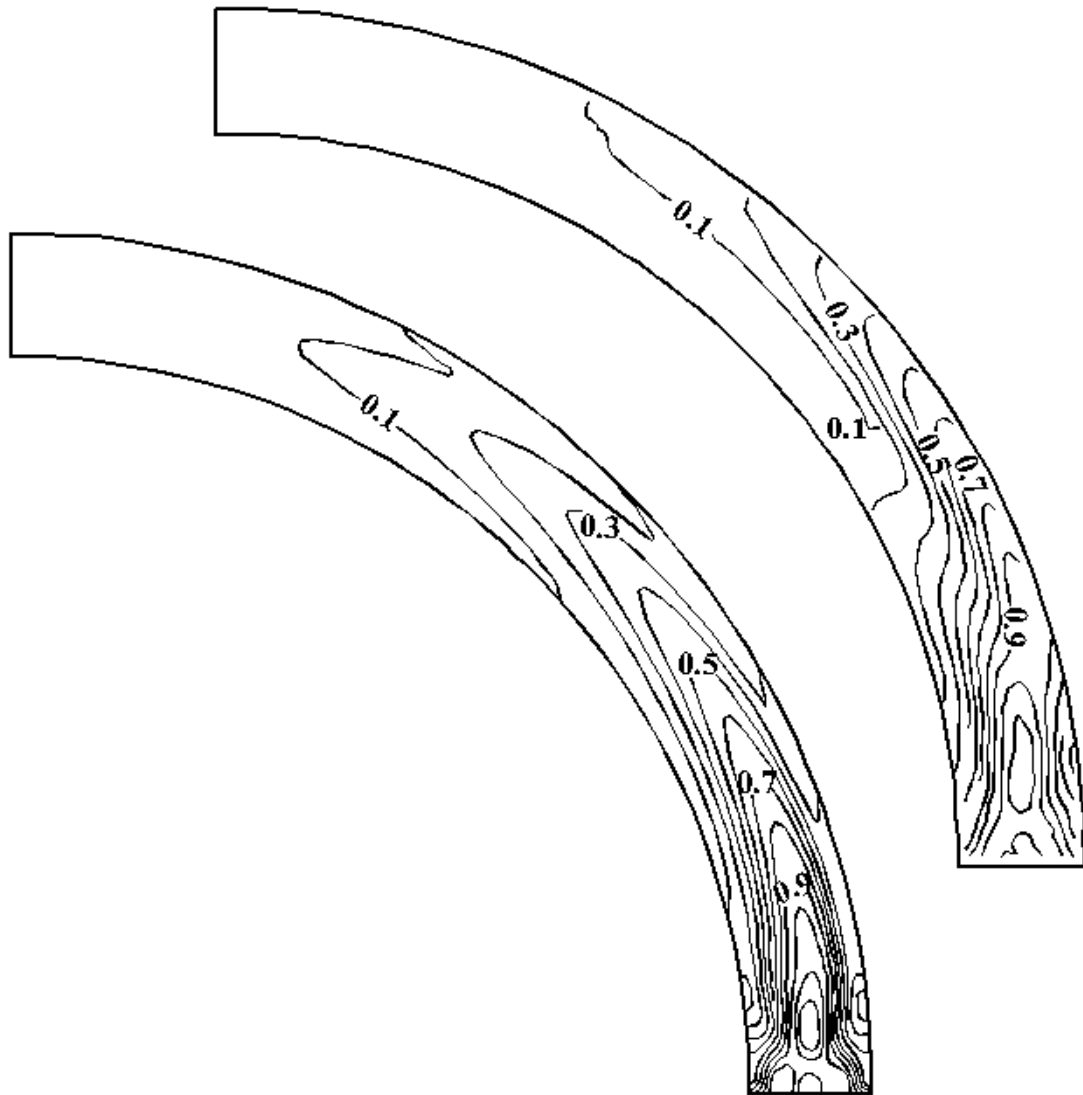


Fig. 23. Wave height comparison in narrow circular channel, with dissipation. (Top: parabolic approximation (Melo and Gobbi 1998); bottom: present elliptic model)

(Reprinted with permission from ASCE.)

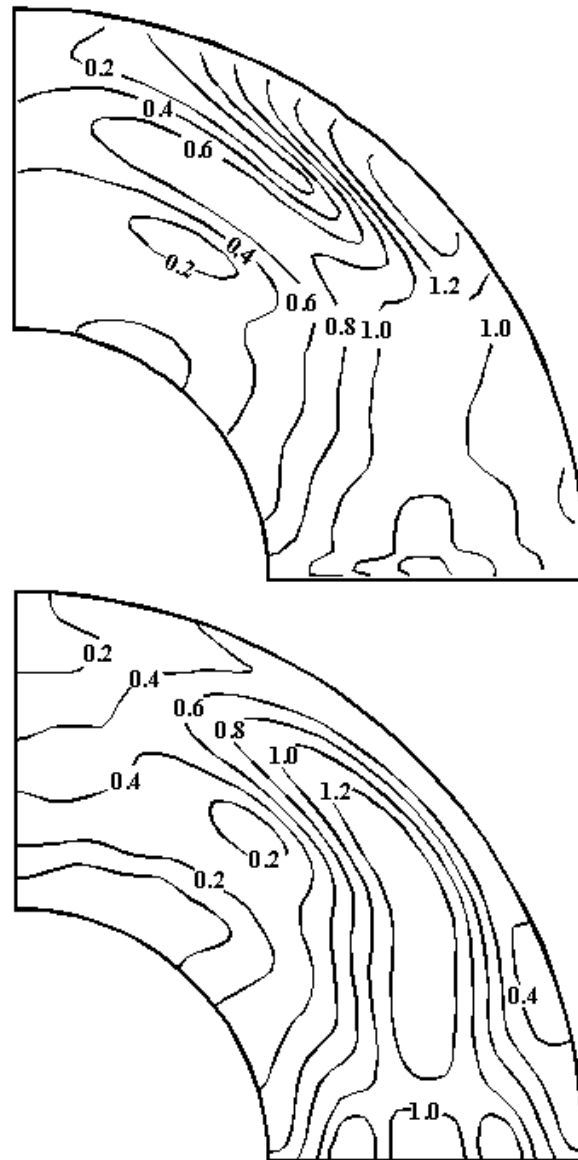


Fig. 24. Wave height comparison in wide circular channel, with dissipation. (Top: parabolic approximation (Melo and Gobbi 1998); bottom: present elliptic model) (Reprinted with permission from ASCE.)

CHAPTER V

SIMULATIONS NEAR POCKET ABSORBER IN PENTWATER HARBOR

In view of the satisfactory results obtained with the modified mild-slope equation (4), it is used to demonstrate the effect of dissipation in a field case. This goal is to examine the performance of the model in a non-idealized situation. A practical harbor problem came to our attention. Pocket wave absorbers (Fig. 1) have been constructed in the entrance channel leading to Lake Michigan near Pentwater Harbor (Thompson et al. 2005) in order to mitigate navigation problems. What's more, a physical model was constructed by the US Army Engineer Coastal and Hydraulics Laboratory. The model study provides some data for model validation. Figs 25 and 26 show the model bathymetry which is patterned after the Pentwater Harbor geometry. In this case, rubble mound structures are present seaward of the coastline as well as in the pocket absorbers.

A numerical model with "Surface Water Modeling System" graphical interface is used to develop the grids. The model domain contains 161,862 nodes. All boundaries were specified as fully-reflecting, but the boundary at the end of the channel is fully-absorbing. To demonstrate the effects of the jetty, we performed simulations with and without friction for normally incident waves of height 1 m and period 5 s. (Fig. 27). It can be seen that without dissipation large waves (blue color in Fig. 27) are created. They may occur in some areas in the channel, in particular, along the south jetty, along the north pocket, and along the north wall down-wave of the pocket absorber (Fig. 27, top panel). However, the rubble mound developed in the channel has dissipative effects and

causes attenuation of these large waves. On the contrary, we observe the overall wave heights on the down-wave side of the pocket absorber are somewhat smaller (more red, less green) when dissipation is applied. A similar reduction in wave heights is also seen outside of the north jetty.

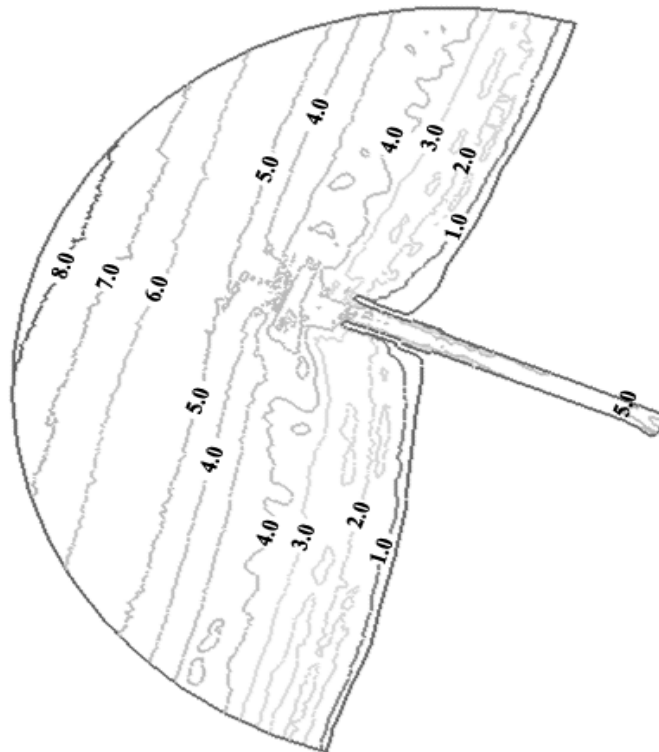


Fig. 25. Pentwater Harbor entrance channel model (depth in m)

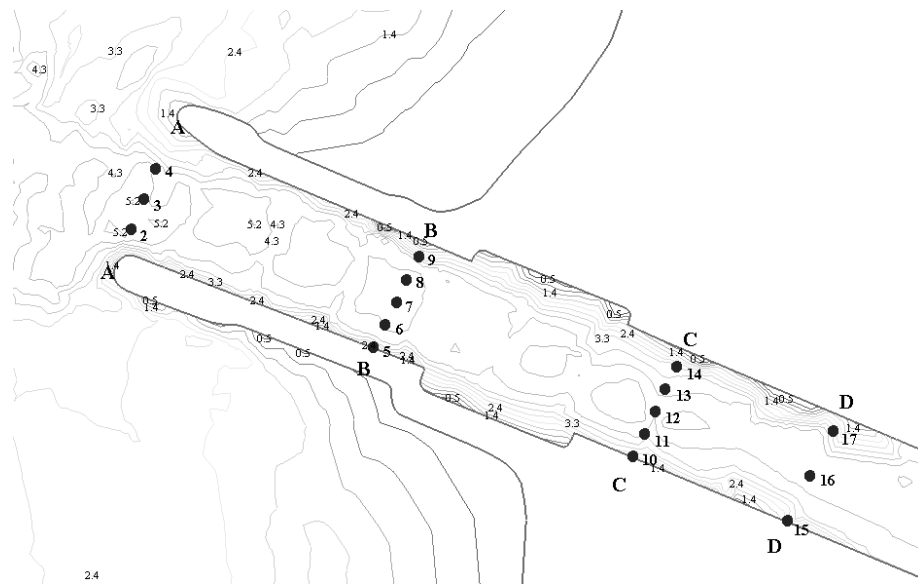


Fig. 26. Pentwater entrance channel, hydraulic model gauge locations (numbered dots) and bathymetry (depth in m)

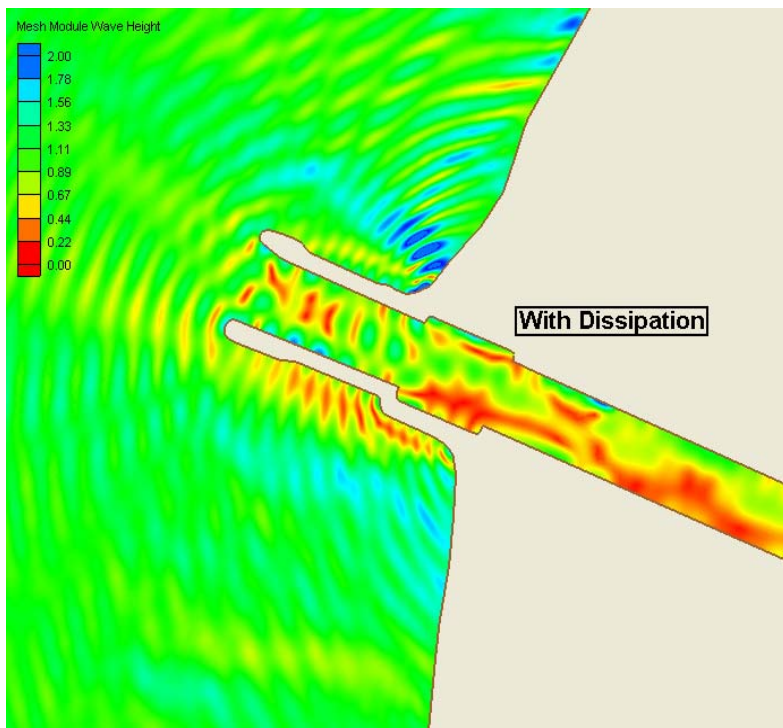
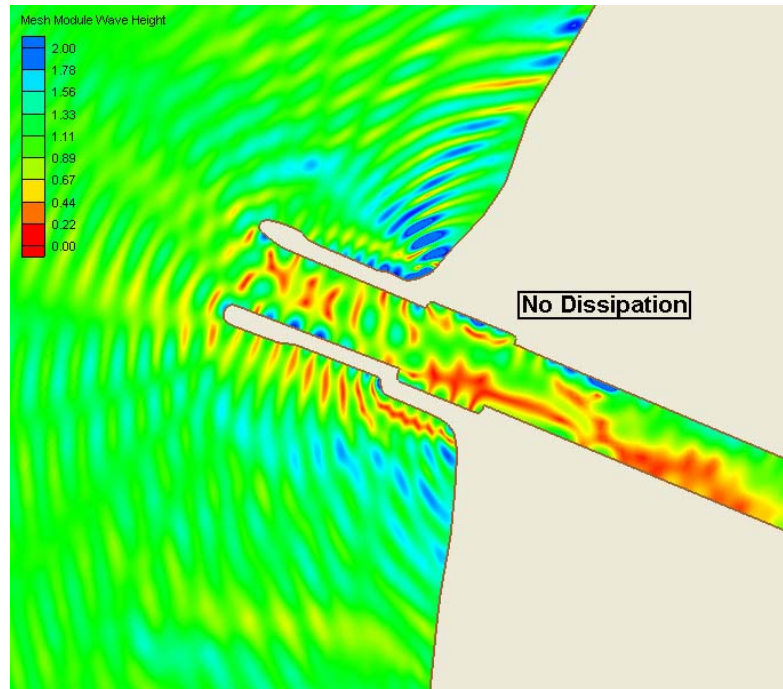


Fig. 27. Modeled wave height comparison

Wave height measurements along four transects (AA, BB, CC, DD) were presented by Thompson et al. (2005). The gauge measurement was employed to record wave heights. Totally, 16 gauges were used and denoted by numbers 2-17 in Fig. 26.

Although the wave-maker generated spectral waves, examination of some of the hydraulic model photographs (e.g. Figs.28 and 29) suggested that a monochromatic representation was acceptable for efficiency of numerical simulation for our purpose. In any case, full details of the incident wave spectrum were not readily available. Simulations for the following cases were performed: (a) incident wave height $H_i = 1\text{m}$, $T = 5\text{s}$; (b) $H_i = 2\text{m}$, $T = 8\text{s}$; and (c) $H_i = 2\text{m}$, $T = 7\text{s}$. Also, incident wave angles of 0° and 45° were considered.

Numerical simulations and hydraulic model photographs are shown for cases (a) and (b) in Figures 28 and 29, for incident wave angles of 0° and 45° respectively. (For case (c), no photographs are available; however, quantitative results are presented later).

In general, the both modeled wave patterns are very similar (also shown in Figs. 28 and 29). A comparison of model results with gage data along the 4 transects (Figs. 30 & 31) suggests the model captures the salient features of the wave patterns reasonably well. In general, the data show wave height attenuation as one goes down the channel; the reduction in the vicinity of transects CC and DD is of the order of approximately 80% and 50% in case (a), and 75% and 30% in case (b). There are some discrepancies, which can perhaps be attributed to the following factors. The overall pattern of the wave field seen in Figs. 28 and 29 is fairly complex in the channel and near the structures, suggesting that more gage measurements may be needed to properly represent the wave-field. Also the incident spectrum was unknown, as was the exact location of the gages. The properties of the rubble mound structure such as the exact width, porosity, etc. were also unknown and our choice of the parameters may influence the comparison.

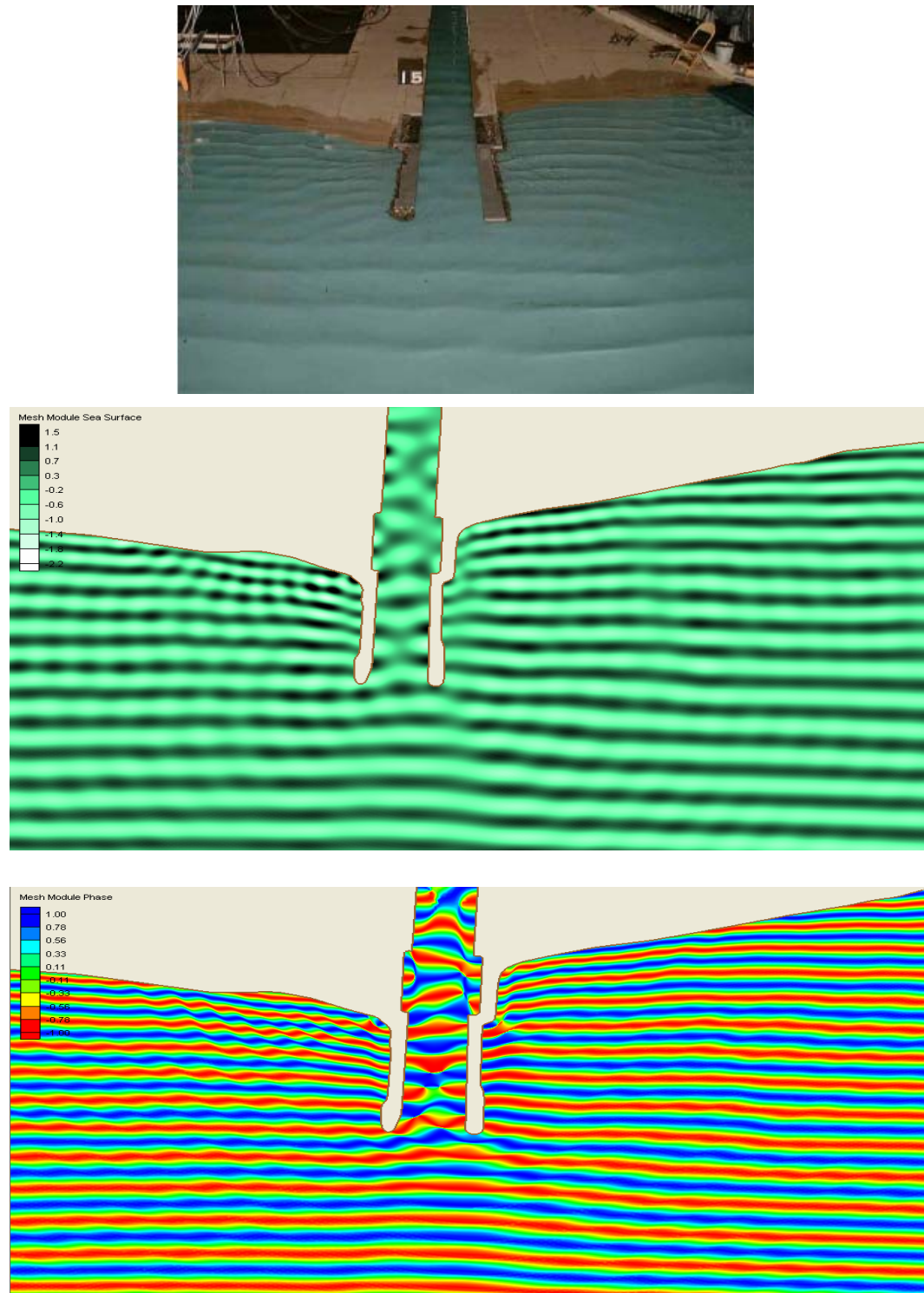


Fig. 28. Hydraulic and numerical model sea surface snapshot (top two panels) and numerical model phase diagram (bottom panel) for normally-incident wave

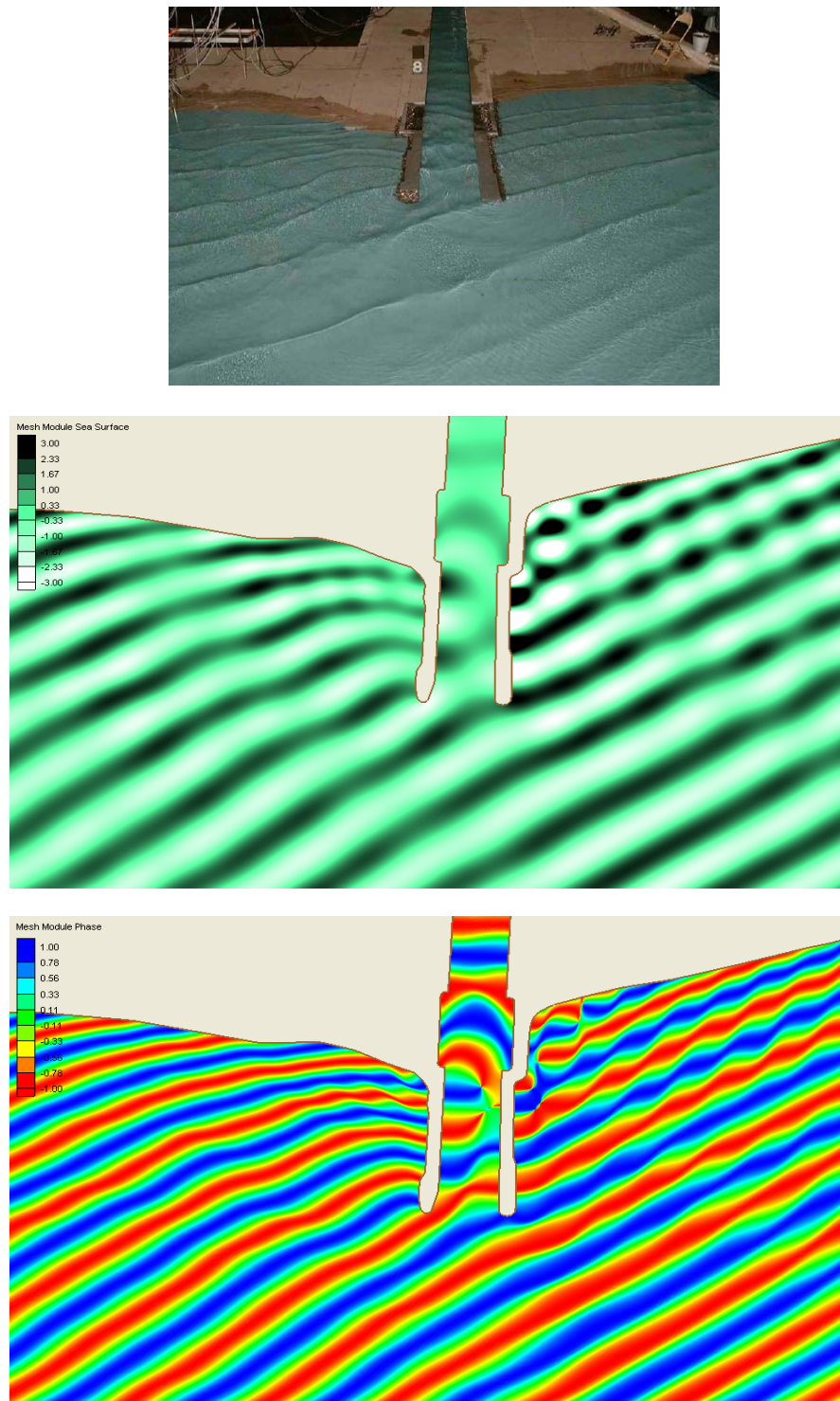


Fig. 29. Hydraulic and numerical model sea surface snapshot (top two panels) and numerical model phase diagram (bottom panel) for oblique wave incidence

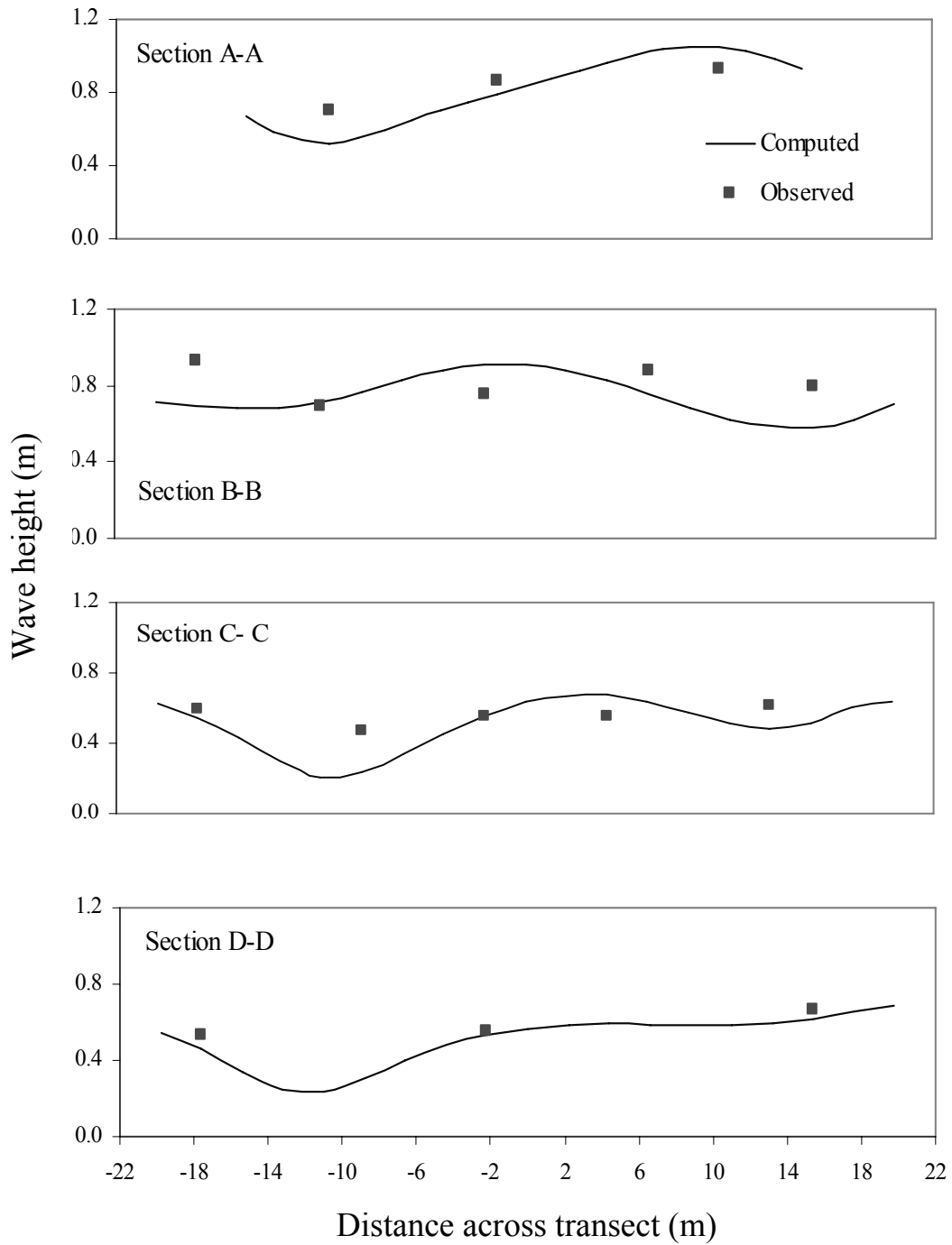


Fig. 30. Wave height comparison, $H_i = 1\text{m}$, $T = 5\text{s}$

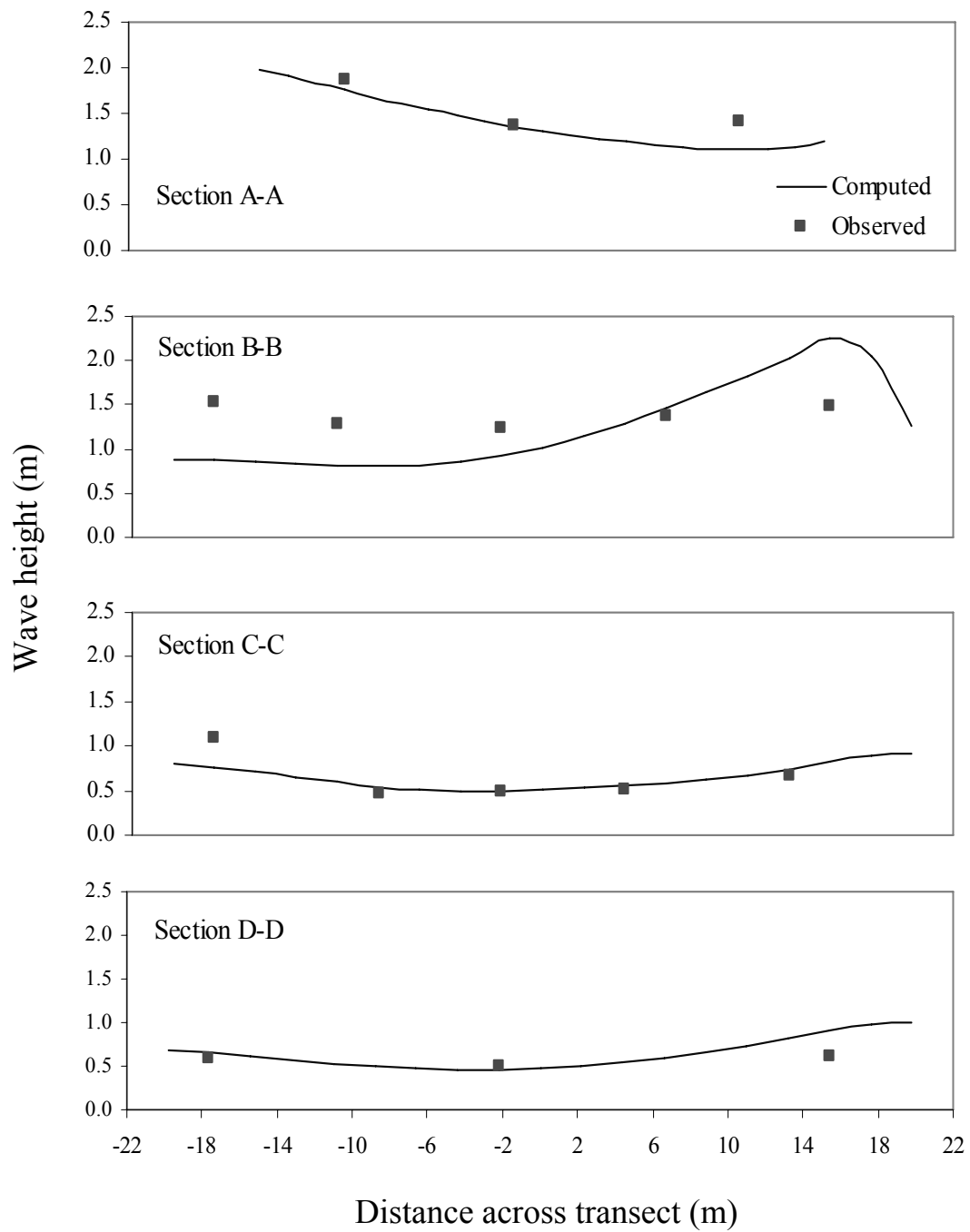


Fig. 31. Wave height comparison, $H_i = 2$ m, $T = 7$ s

Thompson et al. (2005) have noted the absence of guidelines for designing pocket absorbers and have noted that several options can be considered by the designer. Here we examine, for case (a), the effects of eliminating one pocket and of staggering the pockets on either side wall (configurations A and H in Fig. 2). The results (Fig. 32) may be compared with those in Fig. 27 (bottom panel) where two (nearly) symmetric pocket absorbers are included. The wave heights in the entrance channel seem to experience much greater reflection when the two pocket absorbers are staggered (Fig. 32, bottom panel), and surprisingly, the wave heights in the channel resulting from the use of just one pocket are somewhat lower than when two pockets are used.

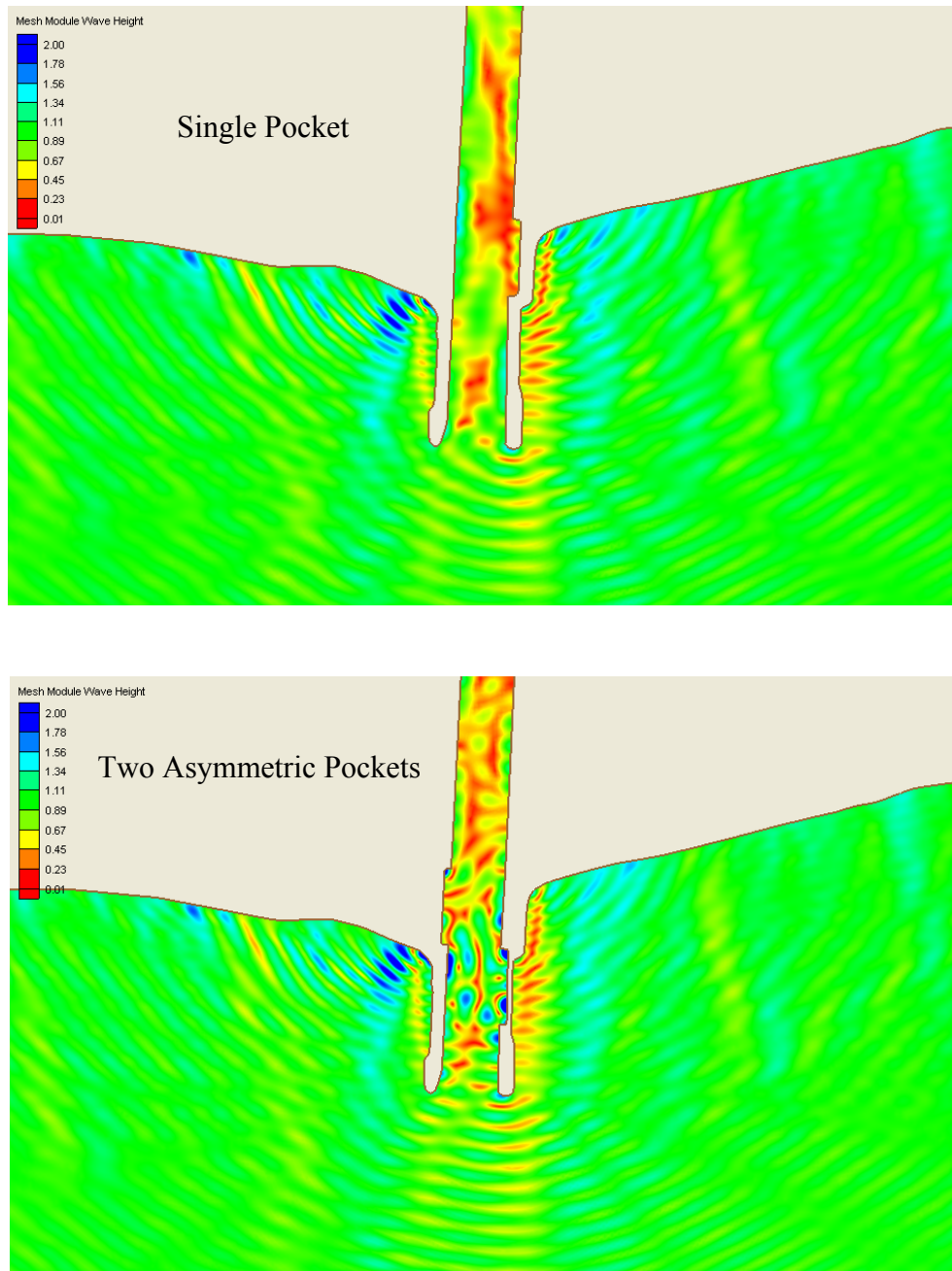


Fig. 32. Modeled wave heights for alternative entrance channel configurations

CHAPTER VI

CONCLUDING REMARKS

The effect of rubble mound structures has been included so far in models based on the parabolic approximation of the mild-slope wave equation (Melo and Guza 1991a; 1991b) or on the three-dimensional Laplace equation (Sulisz 2005). Relative to the elliptic mild-slope wave equation that is widely used in harbor applications, these models have limitations, either in their computational attributes or in their ability to simulate angular scattering. We have therefore explored the incorporation of the related dissipation mechanism in the two-dimensional elliptic equation. Although the dissipation formulation used is essentially the same as in earlier models (based on the Lorentz principle), the iterative treatment of the nonlinearity is fundamentally different.

The resulting model was applied to an idealized pocket absorber (studied by Sulisz 2005) and to straight and curved channels bounded by rubble mound (studied by Melo and Guza (1991a; 1991b) and by Melo and Gobbi (1998)). The model was also applied to a pocket absorber patterned after the Pentwater Harbor entrance (Thompson et al. 2005). For the idealized pocket absorber, the solutions of the present 2d elliptic model match the 3-d solutions of Sulisz (2005) quite well. This test provided model validation against a more complete (three-dimensional) solution. It also shows that the pocket absorbers can create regions of high wave heights on the up-wave side; these reflected waves can potentially be hazardous to small boats. In the case of the straight channel, the results of the parabolic approximation were very similar to the present results. A

good match was also seen in the case of the curved channel when the simulations involved no dissipation. However, when dissipation was modeled, the results of the full elliptic model deviated from those of the parabolic approximation. This suggests that dissipation can increase the angular scattering of waves and be a further impediment to the parabolic models. The elliptic model results also captured, in a qualitative sense, most of the features seen in photographs of hydraulic model simulations of the Pentwater Bay entrance channel. In a quantitative sense, the attenuation measured along transects down-wave of the pocket absorber was largely reproduced. For the Pentwater Bay entrance channel, alternative arrangements for the pocket absorbers were considered as an illustration. The results showed that for the incident wave condition examined, the configuration with one absorber was the most effective in reducing the wave heights.

The above results suggest that the incorporation of dissipative effects as described here can be an effective method of extending the practical utility of existing two-dimensional elliptic harbor wave simulation models. It could help to address the need for design tools as stated by Thompson et al. (2005) in the context of pocket wave absorbers in the Great Lakes region.

REFERENCES

- Booij, N. (1981). "Gravity Waves on Water with Non-uniform Depth & Current." Ph.D. thesis, Technical Univ of Delft, The Netherlands.
- Bova, S. W., Breshears, C. P., Cuicchi, C., Demirbilek, Z. and Gabb, H. A. (2000). "Dual-level Parallel Analysis of Harbor Wave Response Using MPI and OpenMPI." *Internat. J. High Performance Computing Applications*. v14, 1, 49-64.
- Chandrasekera, C. N. and Cheung, K. F. (1997). "Extended Linear Refraction-Diffraction Model." *J. Waterway, Port, Coastal & Ocean Eng.* 123(5), 280-286.
- Chen, H. S. (1986). "Effects of Bottom Friction and Boundary Absorption on Water Wave Scattering." *Applied Ocean Research*. 8(2), 99-104.
- Chen, W., Panchang, V. G. & Demirbilek, Z. (2005). "On the Modeling of Wave-Current Interaction using the Elliptic Mild-Slope Wave Equation.", *Ocean Eng.*, v32, 2135-2164.
- Dalrymple, R. A., Kirby, J. T. and Hwang, P. A. (1984). "Wave Diffraction due to Areas of High Energy Dissipation." *J. Waterway, Port, Coastal and Ocean Eng.* 110(1), 67-79.
- Dalrymple, R. A., Martin, P.A. and Li L. (2000). "Wave in Rectangular Inlet with Reflecting or Absorbing Walls." *J. Waterway, Port, Coastal and Ocean Eng.* 126(6), 288-296.
- Demirbilek, Z. and Panchang, V. G. (1998). "CGWAVE: A Coastal Surface Water

- Wave Model of the Mild Slope Equation.” *Tech Rept CHL-98-26*, US Army Corps of Engineers Waterways Expt Stn, Vicksburg, MS.
- Li, B. (1994). “A Generalized Conjugate Gradient Model for the Mild Slope Equation.” *Coastal Eng.*, 23, 215-225.
- Li, D., Panchang, V. G., Tang, Z., Demirbilek, Z. and Ramsden J. (2005). “Evaluation of an Approximate Method for Incorporating Floating Docks in Two-dimensional Harbor Wave Prediction Models.” *Canadian J. of Civil Eng.*, 32, 1082-1092.
- Melo, E. and Gobbi, M. F. (1998). “Wave Propagation in Circular Jettied Channels.” *J. Waterway, Port, Coastal and Ocean Eng.*, 124 (1), 7-15.
- Melo, E. and Guza, R. T. (1990). “Wave Propagation in a Jettied Channel Entrance.” *SIO Reference Series 90-1, Scripps Institution of Oceanog.*, La Jolla, CA.
- Melo, E., and Guza, R. T. (1991a). “Wave Propagation in Jettied Entrance Channels. I: Models.” *J. Waterway, Port, Coastal and Ocean Eng.* 117(5), 471-492.
- Melo, E., and Guza, R, T. (1991b). “Wave Propagation in Jettied Entrance Channels. II: Observations.” *J. Waterway, Port, Coastal and Ocean Eng.* 117(5), 493-509.
- Okiihiro, M. and Guza, R. T. (1996). “Observations of Seiche Forcing and

- Amplification in Three Small Harbors.” *J. Waterway, Port, Coastal & Ocean Eng.*, 122(5), 232-238.
- Panchang, V. G., Cushman-Roisin, B. and Pearce, B. R. (1988). “Combined Refraction-Diffraction of Short Waves for Large Coastal Regions.” *Coastal Eng.*, 12, 133-156.
- Panchang, V. G., Ge, W., Cushman-Roisin, B. and Pearce, B. R. (1991). “Solution to the Mild-Slope Wave Problem by Iteration.” *Applied Ocean Research*, 13(4), 187-199.
- Panchang, V. G., Chen, W. Xu, B., Schlenker, K., Demirbilek, Z. and Okihiro, M. (2000). “Effects of Exterior Bathymetry in Elliptic Harbor Wave Models.” *J. Waterway, Port, Coastal & Ocean Eng.*, 126(2), 71-78.
- Panchang V. G. & Demirbilek, Z. (2001). “Simulation of Waves in Harbors Using Two-Dimensional Elliptic Equation Models.” *Adv. in Coastal & Ocean Eng.* (World Scientific), 7, 125-162.
- Sulisz, W. (2005). “Wave Propagation in Channel with Side Porous Caves.” *J. Waterway, Port, Coastal and Ocean Eng.* 131(4), 162-170.
- Tang, Y., Ouellet, Y. and Ropars, Y. (1999). “Finite Element Modelling of Wave Conditions Inside Sainte-Therese-de-gaspe Harbour, Quebec.” *Proc. Canadian Coastal Confer.*, Fraser Delta, pp. 737-748.
- Thompson, E. F. and Demirbilek, Z. (2002). “Wave Climate and Wave Response, 2025 Plan, Kahului Harbor, Hawaii.” *USACOE, ERDC, TR-02-21*, Vicksburg, MS.

- Thompson, E. F., Bottin, R. R. and Selegan, J. P. (2004). "Effectiveness of Pocket Wave Absorbers in Vertical-Wall, Coastal Entrance Structures." *Tech Rept ERDC/CHL CHETN-III-69, US Army Corps of Engineers Waterways Expt Stn, Vicksburg, MS.*
- Thompson, E. F., Bottin, R. R. and Shak, A. T. (2002). "Monitoring of Entrance Channel Navigation Improvements at Morro Bay Harbor, Morro Bay, California." *USACOE, ERDC, TR-02-18, Vicksburg, MS.*
- Thompson, E. F., Myrick G. B., Zager N. J., Bottin R. R., Sabol M. A., Selegan J. P., Mckinney J. P., Demirbilek Z. and Acuff H. F. (2006). "Monitoring of Entrance Channel Navigation Improvements at Pentwater, Michigan, and Design Guidance for Pocket Wave Absorbers." *Tech Rept TR-06-3, US Army Corps of Engineers Waterways Expt Stn, Vicksburg, MS.*
- Tsay, T. K. and Liu, P. L.F. (1983). "A Finite element Model for Wave Refraction and Diffraction." *Applied Ocean Research*, 5(1), 30-37.
- Tsay, T. K., Zhu, W. & Liu, P. L.F. (1989). "A finite element model for wave refraction, diffraction, reflection, and dissipation." *Applied Ocean Research*, 11, 33-38.
- Zhao, L., Panchang, V. G., Chen, W., Demirbilek, Z. & Chhabbra, N. (2001). "Simulation of Breaking Effects in a Two-dimensional Harbor Wave Prediction Model." *Coastal Eng.*, 42(4),359-373.

- Zubier, K., Panchang, V. G. & Demirbilek, Z. (2003). "Simulation of Waves at Duck (North Carolina) Using Two Numerical Models" *Coastal Eng.*, 45(3), 439-469.
- Zundel, A. K., Fugal, A. L., Jones, N. L. and Demirbilek, Z. (1998). "Automatic Definition of Two-dimensional Coastal Finite Element Domains." *Proc. 3rd Internat. Conf. Hydroinformatics*. Ed. V. Babovic and L. C. Larsen. A. A. Balkema, Rotterdam, 693-700.

VITA

Jianfeng Zhang received his Bachelor of Science degree in Coastal and Ocean Engineering Department from Hohai University at Nanjing in People Republic of China in 2000. After he graduated from the university, he began his professional career. He worked on coastal structures and harbor design in FHDI Engineering Co., Ltd. for almost four years. And then, he entered Ocean Engineering Program in Civil Engineering Department at Texas A&M University in January 2004, and he received his Master of Science degree in May 2007. His research interests include wave propagation and dissipation near shore and offshore structures. He plans to continue his doctoral degree at Ocean Engineering Program and continues to study wave prediction models.

Mr. Zhang, his permanent address is 47 Lutong Street, Fuzhou 350009, P.R.China. His email address is zjianfeng@msn.com.